Advanced Functional Biotextiles for a Circular Materials Economy

Theanne N. Schiros[1,2]†, Romare Antrobus[3]†, Delfina Farias[1], Yueh-Ting Chiu[3], Christian Tay Joseph[2], Shanece Esdaille[2], Gwen Karen Sanchiricco[1], Grace Miquelon[1], Dong An[4], Sebastian T. Russell[4], Adrian M. Chitu[5], Susanne Goetz[6], Anne Marika Verploegh Chassé[7], Colin Nuckolls[8], Sanat K. Kumar[4], and Helen H. Lu[2]**

[1]Department of Science and Mathematics, Fashion Institute of Technology; New York, NY 10001.

[2]Materials Research Science and Engineering Center, Columbia University; New York, NY 10027.

[3]Department of Biomedical Engineering, Columbia University; New York, NY 10027.

[4]Department of Chemical Engineering, Columbia University; New York, NY 10027.

[5]Materials Science and Engineering, Columbia University; New York, NY 10027.

[6] Surface/Textile Design, Fashion Institute of Technology; New York, NY 10001.

[7]Footwear and Accessories Design, Fashion Institute of Technology; New York, NY 10001.

[8]Department of Chemistry, Columbia University, New York, NY 10027.

†These authors contributed equally to this work.

*Co-corresponding authors. E-mail: ts2526@columbia.edu, hhlu@columbia.edu

Keywords: microbial biofabrication, biotextiles, flame-reardance, LCA, circular economy

Abstract: A circular materials economy can disrupt linear production models and mitigate its environmental threats. We harness extracellular biosynthesis of microbial nanocellulose (MC), coupled to a protocol that represents a serendipitous intersection between ancient textile techniques and green processing as a route to high-performance bioleather with a circular life cycle. Specifically, a plant-based lecithin phosphocholine treatment modulates cellulose cross-linking through phosphate and methylene groups, to yield a biodegradable material with superior mechanical and flame-retardant properties. A broad color palette and controlled color modulation was achieved with cultural heritage dyes and waste-to-resource strategies. Life cycle impact assessment shows up to an order of magnitude reduction in environmental impacts relative to conventional textiles, making MC relevant for widespread application in fashion, interiors, construction and insulating materials. The translational

potential of this approach is tremendous, as use of microbes and green chemistry to engineer regenerative, high-performance products can accelerate a paradigm shift to a circular bioeconomy.

1. Introduction

The linear economy that has been the dominant production model since the Industrial Revolution drives climate instability and threatens ecological and human health. The textile industry, in particular, is reliant on industrial agriculture for cellulosic fibers,[1] nonrenewable petrochemicals to produce synthetic fibers, dyes, tanning and finishing agents, and chemically and energy intensive processing.[2] It is responsible for 10% of global carbon emissions, [3] 20% of global waste water, [4] 35% of marine microplastic pollution, [5] and expected to use 25% of the global carbon budget by 2050.[6] For instance, the cattle industry is the single leading driver of deforestation, [7] while chrome tanning leather creates large volumes of mutagenic, teratogenic, and carcinogenic chemical pollution, such that tannery effluents rank as the highest pollutants among all industrial wastes.[8] Leather alternatives created from petrochemical-based textiles and coatings have emerged. However, these materials are not biodegradable, contain endocrine-disrupting chemicals, and shed nano- and micro-plastics, which absorb and accumulate persistent organic pollutants. Microplastics have been found in the intestines of marine animals and humans, and, recently, in human placenta.[9-10] Thus, there is a pressing need for new fabrication strategies that minimize and close material and energy loops in a regenerative, circular economy, to make industrialization compatible with nature and sustainable global development.

This challenge has motivated a search for more sustainable, bio-based textiles, especially leather alternatives, [11] including mycelium and pineapple leather, and gene editing of yeast to produce collagen. Microbial nanocellulose (MC) is a highly crystalline biopolymer produced extracellularly by bacteria, one of the most promising in terms of cellulose yield being *Acetobacter xylinus*.[12] Under aerobic conditions, these bacteria biosynthesize extracellular cellulose nanofibrils (10–100 nm diameter) that self-assemble into a three-dimensional layered pellicle with high water content (>98%) at the air-media interface under static conditions.

The bottom-up assembly of MC offers unique advantages to tune and meet key design criteria—rapid renewability, low toxicity, scalability, performance, and compostability—for multi-functional, circular economy textiles. Although identical in chemical structure to plant-based cellulose, MC is distinctly characterized by its readily extractable nanofiber network,

degradability, excellent tensile strength due to high degrees of polymerization and crystallinity (80-90%), and the possibility to control these and other physical properties including porosity during biosynthesis.[13] Importantly, MC can offer a rapidly renewable raw material while eliminating the land, water and chemicals usage of production of agricultural[14] and wood pulp cellulose.[15] For instance, the amount of cellulose produced by eucalyptus in a 10,000 m^2 area of land over 7 years could be achieved at higher purity by microbial fermentation in a 500 m^3 bioreactor in 22 days.[16]

However, like many naturally occurring biopolymers, including the aforementioned bio-based leather alternatives, the hygroscopicity of as-fabricated MC results in unstable mechanics that hinders translation to textile applications.[17] Strategies to improve the mechanical and moisture stability of "bioleathers" typically involve heavy metals and/or synthetic plasticizers and coatings which compromise material biodegradability, introduce human and ecological toxicity, and increase flammability,[18] making development of innovative green processing a major research priority.

Yet, for millennia, societies around the world have created durable, water-repellent leather using non-toxic tanning methods, including brain and organ tanning followed by smoke tanning, dating back at least 5,000 years to "Ötzi" (Iceman).[19] Unfortunately, much of these ancient methods have been lost, and the chemical mechanism of fat tanning is not fully understood. It has been proposed that braining and smoking hides are forms of aldehyde tanning, in which the aldehyde carbon reacts with the amine nitrogen of collagen to produce an imine product, which reacts with an amine on a neighboring polypeptide to covalently cross-link the collagen into leather.[20] Brain tissue is high in fatty acids and lecithin. The lipid portion of lecithin molecules polarize away from water in the emulsion, while the phosphate and choline groups are attracted to it, stabilizing the tanning emulsion and facilitating interaction between the oils and collagen.

Inspired by these ancient practices, we hypothesize that lecithin phosphatidylcholine will modify the cross-linking and material properties of MC through its hydrophilic -OH groups to make it suitable for use as a bioleather. An increase in ductility of MC with application of traditional brain and smoke tanning processes provided a positive control to further encourage this line of investigation (Figure S1). Following a bottom-up approach of microbial biosynthesis of nanocellulose coupled to a plant-based lecithin tanning emulsion, we create a high performance bioleather that exhibits high tensile strength, ductility, and outstanding flame retardance, and soil biodegradability (**Figure 1**). Here, a symbiotic colony of *Acetobacter* and yeast (SCOBY) metabolizes sugars into cellulose nanofibers via

enzymatic pathways.[13] A variety of carbon sources, such as glucose, fructose, and sucrose, which may be extracted from agro-industrial by-products, can be utilized for scalable production of MC (Movie S1). A range of colors and design motifs are achieved using historically important natural dyes and waste-to-resource strategies, offering a non-toxic alternative to the brown color resulting from the Maillard reaction when MC is produced in a SCOBY. Tailoring the shape of the cultivation vessel to the pattern geometry enables zero waste production, as shown for our biodegradable, bioleather bag prototypes (Figure 1). The microbial bioleather created here meets key criteria for a circular material economy, including renewability, low toxicity, functional and environmental performance, biodegradability and scalability.

2. Results and Discussion

2.1. Physical and Mechanical Properties with Lecithin Phosphocholine Treatment

We investigate the effect of lecithin treatment on MC, as well as an aldehyde smoke treatment, as documented for brain tanning of hides in order to complete the conversion to leather. As-fabricated, lecithin "tanned", aldehyde tanned (smoked), and lecithin and aldehyde tanned MC are denoted MC, LT, S, and LTS, respectively. A dense, three-dimensional network of unaligned, intertwined nanofibers is observed with scanning electron microscopy (SEM) on MC surfaces before and after processing (**Figure 2A**). Treatment with lecithin and aldehyde tanning, separately and sequentially, yields no significant differences in fiber size relative to as-fabricated MC (average diameter of 71.00 ± 19.00 nm, Table 1). This indicates that the emulsion does not coat the fibers but is rather removed with rinsing. However, compositional analysis with energy dispersive x-ray measured nearly four times higher phosphorous concentration than the MC control (2.02% vs. 0.57%, ^$p<0.05$, $n=3$), supporting the hypothesized favorable interaction between the phosphocholine group of lecithin with cellulose (Figure S2).

Common to unprocessed biopolymers, as-fabricated MC samples exhibit varied stress-strain profiles under uniaxial tensile testing (**Figure 2B**). The typical trade-off between tensile strength and ductility, the latter a reflection of flexibility which considers both the strain at yield point and toughness, is apparent for dried MC. Despite the same biosynthesis and processing parameters, MC exhibits elastic moduli ranging from 58.30 ± 35.71 to 210.91 ± 58.61 MPa for MC1 (high tensile strength, brittle) and MC 2 (lower tensile strength, greater ductility), respectively (**Table 1**). Without lecithin treatment, smoked (S) samples also have

variable mechanical properties. Lecithin tanning stabilizes the mechanical properties and increases the elastic modulus, toughness, and maximum stress (^ $p<0.05$, $n=4$) of the material; LT group exhibits higher tensile strength than leather or cotton up to strain values of 33% and 45%, respectively (Figure 2B). Surprisingly, the superior mechanical properties of LT are not reflected in the bulk microstructure as probed with x-ray diffraction (**Figure 2C).** The (1-10), (110) and (200) Bragg peaks of cellulose I are largely unaffected by lecithin tanning, with only a minor increase in crystallinity index (87% vs 84%, Table 1), calculated using a peak deconvolution method,[21] and unchanged d-spacing and similar crystalline domain size relative to MC (Table S1). A similar increase in tensile strength and ductility unaccompanied by changes in microstructure has been observed for phosphorylated cellulose with low phosphorus concentrations comparable to those measured for LT.[22]

2.2 Flame retardance due to lecithin tanning and unique self-organization of MC nanofibers

Flame-retardance is an important design criterion for performance textiles, but industrial flame-retardant chemicals are considered hazardous substances linked to autoimmune diseases, learning disabilities, neurological and reproductive problems, birth defects, and cancer.[23] Since phosphorous compounds are effective in reducing biopolymer flammability,[24] phosphorylation with LT prompted investigation of MC biotextile flame retardance. Remarkably, when exposed to a direct 2054° C flame, LT biotextiles do not ignite (**Figure3A**). After 40 seconds, a control aluminum brazing rod is introduced and melts within seconds of application of the flame, while the biotextile continues to deflect the flame, without propagation. When LT samples are repeatedly exposed to the direct flame until surface char is formed, the bulk LT biotextile is observed to be intact just below the easily removable surface char, underscoring its outstanding flame-retardant capacity (Figure3A).

Analysis of the thermal stability and decomposition behavior of as-fabricated and treated biotextiles provide insights on the mechanism of flame retardance. Thermogravimetric analysis (TGA) and dTGA curves (**Figure3B**) show a three-step mass loss, representing: (I) the initial evaporation of free and bound water between 25-200°C; (II-III) polymer decomposition (210-240°C); and (IV) the production of either pyrolysis-based levoglucosan or flame-resistant char (300-360°C). Higher mass loss is observed for LT relative to MC in regions I-III: 8.50±0.25% vs 5.38±0.87% at 150 °C (region I); 29.55±0.25 vs 16.96±2.37% at 232 °C (region II) and 58.99±0.55% vs 49.51±1.21% at 340°C (region III). Finally, a lower decomposition temperature onset is also observed for L, and aliphatic compounds are

decomposed into char with a greater residual mass for LT than MC at 680°C (18.18% vs 8.99%).

The data indicates that lecithin treatment lowers the decomposition temperature of MC and redirects the combustion pathway from formation of levoglucosan towards formation of foaming char as an insulating oxygen barrier, resulting in the outstanding flame resistance. This is attributed to the addition of phosphorous compounds with lecithin tanning, which promotes dehydration to yield unsaturated compounds that polymerize at high temperatures to a cross-linked, intumescent foaming char. Notably, as-fabricated MC also demonstrates a degree of flame retardance, which may be a consequence of the nanoscale self-organization of MC fibers into a layered structure, visible under the deflected flame (Figure 3A). To investigate the influence of the layered microstructure on flame retardance, as-fabricated MC samples of varying thickness (obtained by removing layers from a hydrated MC pellicle (45 cm x 54 cm, 2.5 cm thick, Figure S3)), dried under ambient conditions, are flame tested (**Figure 3C**). The mass loss to combustion decreases with increasing MC thickness until 2.5 cm, beyond which point MC material loss is minimal, although greater than for LT biotextiles of the same thickness (Figure 3A, C).

The formation of intumescent bubbles on the nanofiber surface exposed to the flame is observed in the charred portion of LT, as well as for untreated MC of sufficient thickness (≥ 2.5 cm), in high magnification SEM images (**Figure 3D**). The multi-layer structure of MC mimics that of a multilayer nanocoating, well known as physical surface barriers that limit heat and oxygen transfer between the fire and cellulose, while the densely packed arrangement of MC nanofibers further limits oxygen available to support a flame. Bubble formation is accompanied by generation of water vapor, which favors production of an insulating foaming char barrier, that in turn, prevents combustion by reducing heat transmission to the MC surface, and inhibiting oxygen and combustible volatiles from diffusing to the flame.

To further investigate the effect of the layered structure of MC on flame response, we attempted to disrupt it by blending MC into a slurry and casting it into a film. We note that the MC nanofiber morphology drives self-assembly into a hydrogen-bonded sheet during dehydration without chemical intervention. Surprisingly, while combusting more readily than as-fabricated MC, cast MC films also demonstrate a degree of flame resistance. Electron micrographs of the cross-sections of the films reveal that blended MC *self-organizes to recover the original layered structure* with the nanofiber morphology intact (Figure S4). Thus, in contrast to the ignitable behavior of plant-based cellulose, the unique nano- and

microscale assembly of MC, and in the case of LT, modified chemical properties, imbue the material with non-toxic flame retardance.

2.3 Chemical mechanism underlying improved mechanical performance

Molecular level insights on the chemical origin of the improved mechanical properties for LT biotextiles are revealed by x-ray photoelectron (XPS) and Fourier transform infrared (FTIR) spectroscopy. A peak centered at 134 eV in the phosphorous (P 2p) XPS (Figure4A) indicates that lecithin tanning introduces phosphorus in oxidized states. Carbon 1s XPS reveals an increase in carboxyls, esters and anhydrides, observed at binding energies of ~286.6 (C-O-H), 288.1 (C-O-C), and 289.1 eV (–COOR), respectively.[25] These chemical groups, along with P=O (530.9 eV) and C-O-P bonds (533.5 eV), [26] also modify the O 1s XPS after lecithin tanning (**Figure 4A**).

Chemical fingerprints of bonding observed with FTIR provide mechanistic insights on modulation of cellulose cross-linking with lecithin tanning (**Figure 4B**). New peaks representative of phosphated cellulose appear for LT, including P=O resonances at 1207.4, 1230 and 1252 cm^{1}, and a -P-OH stretch vibration at 898 cm^{-1}.[26-28] Further, enhancement of -OH vibrational peaks characteristic of the cellulose skeleton at 3450-3000 cm^{1} and 664 cm^{-1}, and methyl and methylene resonances, including C–H vibrational bands at 1437-1245 cm^{-1} and 3000- 2853 cm^{-1} and the C–H deformation (1428, 1370 and 1316 cm^{-1}), CH_2 (1184-1104 cm^{-1}) and C-O-H groups (690 cm^{-1}) is observed for LT relative to MC.[27-29)] FTIR peak ratios, expressed as the Lateral Order Index (LOI),[30] shows a higher degree of overall order for LT compared to MC throughout the bulk of the material (Table S4, Figure S5).

Collectively, the data suggests that the lecithin-phosphatidylcholine treatment modifies cellulose cross-linking through phosphate, exocyclic CH_2 and carboxyl groups at well-defined binding sites; proposed mechanisms for these chemical groups are shown schematically (left to right, Figure 4B inset). Methylene groups may form upon reaction with the hydroxyl group at the 6 position (Figure 4B inset), which can react ten times faster than the other -OH groups.[31] Further, carboxyl groups observed with XPS can form ester bonds with hydroxyl groups, which are stronger than the hydrogen bonds of the unmodified cellulose fibers. Low phosphorous concentrations (Figure S2) and unchanged lattice parameters (Table S1) indicate far fewer links are made than hydrogen bonds broken. Indeed, probing the hydrogen-bond intensity in cellulose with FTIR absorbance ratios at different wavelengths, using the C-H stretching band as an internal standard,[32] shows a clear decrease number of intermolecular hydrogen bonds for LT (Methods, Table S2). This supports our

claim that chemical cross-links through methyl, phosphate, and carboxyl bridges form at the expense of hydrogen bonding physical cross-links. This implies that the net strength is higher because of these tighter cross-links (Figure 4B inset), which is confirmed by the higher average modulus (196.4 vs 134.6 MPa) for LT vs MC. The stabilization and improvement of mechanical properties with LT may therefore be attributed to disruption of intrinsic hydrogen bonds between cellulose chains at reactive hydroxyl, methyl and phosphate group sites, leading to an increased interaction between cellulose chains that effectively transfers and distributes applied stress. Additionally, the unprecedented flame retardance promoted by incorporation of phosphates may also be enhanced by the addition of methyl groups with lecithin tanning, which can decrease the rate of combustion by promoting cross-linking during pyrolysis.

2.4 Coloration with Natural Dyes

Color is a feature vital to the commercial success of textiles, and one which currently comes at a high cost of toxicity through use of synthetic dyes.[2.4] Natural dyeing is one of the most ancient of arts, dating back to ~4000 BC Mesopotamia. Leveraging the high biosorption capability of MC,[12] we color microbial biotextiles with natural dyes, including important historical dyes, such as madder, cochineal, and indigo, as well as extracted from waste, including discarded onion skins and nails, which provide tannins and iron acetate, respectively, that bind plant chromophores to cellulose and modify color (**Figure5**). Surface treatment with heated soy wax adds texture and water repellency to the biotextiles (Figure 5.15-16, Movie S2). Surface design motifs, including texture and spatial control in coloration, utilizing ancient folding and printing techniques, denoted Shibori and Hapa Zome in Japan and Adire in West Africa, are demonstrated (Figure 5.17, 5.22), as well as our bioleather sneakers and wallet prototypes (Figure 5.21-5.22).

2.5 Ecological and Human Health Impacts of Microbial Biotextiles

A cradle-to-gate life cycle impact assessment (LCA) is used to compare the environmental and human health impacts of LT biotextile production with the manufacture of conventional textiles, including chrome-tanned leather, synthetic leather (polyurethane (PU)-coated polyester), and cotton canvas (**Figure 6**). For direct comparison, normalization[33] and weighting factors[34] are used to convert the manufacturing impacts across eleven categories into a single score in units of milliPoints (mPts)/m^2 of textile (Table S3); one point (Pt) represents an average individual's annual share of the total environmental impact in the

United States. LT biotextiles biosynthesized in the lab or processed from by-products are denoted $biotextile_{LAB}$ and $biotextile_{BP}$, respectively.

MC biotextiles offer a significant improvement in environmental performance relative to the other fabrics, especially cow leather, which has the largest total impact of the textiles considered (**Figure 6A**). The dramatic impact reduction relative to leather is overwhelmingly due to mitigation of the human toxicity caused by chromium VI derivatives in chrome-tanning, specifically carcinogenics, which account for 95.2% of leather's total impact (Figure 6A, Table S3). Notably, variants of the lecithin tanning were common pre-Industrial methods of tanning hides, and are still used today, but the process only mechanically softens the hide and requires an additional step to modulate cross-linking in collagen to complete the conversion from hide to leather, usually achieved with an aldehyde (smoke) treatment.[35]

Although two orders of magnitude lower than for cow leather, human toxicity is also the largest impact category for $biotextile_{LAB}$. Refinery processes for sugar, the carbon source in the microbial fermentation media, dominate this impact hotspot, the toxicity deriving from carcinogenics and hormonally active agents (**Figure 6B**). This finding motivated us to investigate the potential benefit of sourcing MC as a by-product of commercial food and production, in the form of SCOBY pellicles from a local kombucha brewery ($biotextile_{BP}$). After cleaning, lecithin processing and drying, $biotextile_{BP}$ displayed high tensile strength and ductility, comparable to $biotextile_{LAB}$ (Methods, Figure S7).

Elimination of the fermentation media - and the corresponding agricultural and processing impacts— for MC biotextiles yields a 94% reduction in human toxicity (0.01 vs 0.16 mPts) and a 58% reduction in carbon emissions (0.37 vs 0.89 kg CO_2-eq./m^2) for $biotextile_{BP}$ compared to $biotextile_{LAB}$ (Figure 6A). Critically, the fermentation media not only accounts for ~67% of the total impacts (0.1 vs 0.3 mPts) of MC biotextiles, but also 30-65% of the cost of industrial MC production.[36-37] Thus, the ability to source MC, as well as nutrients for the biosynthesis media, from agro-industrial waste streams opens opportunities for advanced, functional biotextiles with improved circularity and commercial viability.

$Biotextile_{BP}$ mitigates the toxicity of cow leather by a factor of 10^3, and the carbon footprint of synthetic leather and cotton by 96.8% and 94.3%, respectively (0.37 vs 11.50 (PU leather) and 6.5 (cotton) kg CO_2-eq./m^2). Notably, the Ecoinvent data used to model leather assumes hides are a by-product of milk and meat production. As such, the assessment does not include the large climate impacts of the livestock industry,[38] and the LCA shows a minimal carbon footprint for leaher (1.17 kg CO_2-eq/m^2) compared to the other textiles (Figure 6). When modeled as a co-product of the livestock industry, with a portion of cattle

raising and slaughterhouse inputs and outputs included in the LCA scope, the impacts of leather manufacture increase by two orders of magnitude (128 kg CO_2-eq./m^2 and 989 mPts/m^2 total impact (Methods, Table S4).

Finally, we compare the impacts of in situ coloration of MC biotextiles with yellow onion skins obtained as food by-product/waste (Figure 5.7), with impacts reported with synthetic dyeing and finishing of cotton. This simple natural process eliminates 348.13 kg TEG ecotoxicity, 0.18 kg C_2H_3Cl eq. human toxicity, and 5.4 kg CO_2-eq. of climate impacts from synthetic dyeing and finishing, based on data from Murugesh *et. al.*.[39]

2.6 Biodegradation in Natural Terrestrial Environment

Disposal of leather and synthetic leather waste is a serious problem as both are non-biodegradable by microorganisms, while land co-disposal and incineration produce greenhouse gases and introduce carcinogens and other toxins to the ecosystem. In contrast, MC is expected to degrade once exposed to environments rich with cellulolytic microorganisms that hydrolyze the β-1,4-glycosidic linkages of cellulose. To investigate environmental degradability of LT biotextiles, samples (n=5) were weighed and buried at a depth of at least 2.5 cm in tested, nutrient rich soil. After 60 days, with temperatures between 14.2° and 3.2° C, LT showed significant visible deterioration, crumbled easily, and had lost 74.45 ± 2.94 % of the initial mass in the natural environment (Table S8). The data confirms that MC-based products may rapidly reenter the ecosystem, where they may promote the CO_2 capture potential of healthy soil.

3. Conclusions and Future Outlook

We harness microbial biofabrication of nanocellulose and draw inspiration from ancient textile techniques to inform the development of sustainably engineered biotextiles with a circular life cycle. The unique molecular self-organization of MC is combined with bio-phosphorylation with lecithin phospholocholine to create bioleather with high tensile strength, ductility and outstanding flame retardance. This biofabrication approach eliminates the use of hazardous substances, such as chromium VI derivatives for tanning, halogen compounds for fire-retardancy, phthalates as plasticizers, and azo dyes for color. Life cycle assessment quantifies up to an order of magnitude reduction in total environmental damage for lecithin-treated biotextiles relative to conventional textile manufacture, and highlights how use of waste-to-resource strategies can further mitigate impacts. In particular, our bioleather

prototypes mitigate the toxicity of chrome-tanned leather by a factor of 10^3 and the carbon footprints of synthetic leather and cotton by an order of magnitude.

Future prospects include MC-based alternatives to cotton and synthetic fibers as well as conductive, biomedical and sensor textiles.[36] Beyond textiles, phosphorylated biopolymers, including MC, show high performance for diverse applications, from heavy metal pollution remediation to tissue cell engineering and bone regeneration,[40] but the many potential benefits are offset by the toxicity and non-renewability of reagents and high temperatures of conventional phosphorylation processes. The lecithin process developed here may therefore help meet the challenge of developing efficient green manufacturing routes for biopolymers to realize their full potential in a regenerative bioeconomy.

The translational potential of MC is tremendous, as the use of microbes to direct biomaterial formation in a bottom-up process to fabricate high performance products can strategically eliminate the toxicity, water and plastic pollution, and climate impacts of traditional manufacturing processes. Thus, advances in microbial cellulose performance incentivizes a transition to a circular economy, characterized by rapidly renewable resources, waste-to-resource strategies, low impact processes, scalability, and biodegradability.

4. Experimental Section/Methods

4.1 Biosynthesis of microbial cellulose pellicles

Microbial nanocellulose (MC) pellicles were prepared in culture media containing 5.8 w/v% sucrose, 2% w/v green tea as a nitrogen source, and Symbiotic Colony of Bacteria and Yeast (SCOBY) obtained from Fermentaholics © or provided by OM Champagne Tea, a commercial kombucha beverage facility. Culture media was inoculated with 10 w/v% SCOBY starter culture consisting of a combination of bacteria and yeast. Static fermentation at room temperature was maintained until a pellicle at least 2 cm thick was formed at the air-liquid media interface. Biofabrication proceeds as 2-D layer by layer production of a cellulose biofilm which takes the shape of the fermentation vessel. Formed pellicles were washed three times with deionized water to remove residual sugars and air dried for 72 hours at room temperature.

As a post-production treatment, hydrated pellicles were immersed in a lecithin emulsion for 24 hour (LT MC). The lecithin emulsion (LT) consisted of 5% w/v lecithin powder (soy or sunflower seed, 97% phosphatidylcholine) created as a byproduct of the edible oil industry,

and a 20% v/v sunflower seed oil in water and blended at high speed for 60 seconds to create an emulsion.

Microbial nanocellulose samples were also processed following traditional braining tanning practices; the increased mechanical performance for brained tanned MC provided a positive control to investigate the effect of lecithin tanning. A calf brain was purchased from Esposito Meat Market, New York, NY, and processed into an emulsion with a blender. The brain emulsion was rubbed into the MC surface, left for two hours, and then rinsed.

Dehydrated MC samples treated with and without lecithin tanning, were then exposed to an additional smoke tanning aldehyde treatment, in which biofilms were placed into a hydrocarbon-rich environment for 1 hour, using a Smoke Hollow 26142E 26-Inch Electric Smoker with Adjustable Temperature Control and Kingsford smoking wood chips, with the temperature between 160° and 210°F. Prolonged exposure of the MC biotextiles to hydrocarbon-rich smoke was investigated as a mean to seal in the lecithin and oils, which has been documented to traditionally follow brain tanning.

4.2 Characterization

4.2.1 Scanning Electron Microsopy (SEM). Microbial cellulose morphology was assessed by using a scanning electron microscope (Zeiss Sigma VP, Oberkochen, Germany; 3 kV; n=5). Briefly, hydrated microbial cellulose samples were initially placed in a -20ºC freezer for 24 hours and lyophilized in a freeze dryer system (Labconco FreeZone, Kansas City, MO, USA) for 24 hours at −84 °C and 2.0×10^{-2} mbar. Prior to imaging, samples were sputter coated (Cressington 108, Watford, UK) with 30 nm of gold. The fiber diameter of each sample was measured by analyzing randomly selected fiber segments in SEM images using NIH ImageJ software (Bethesda, MD, USA; n=100), to calculate an average fiber diameter.

4.2.2 Water contact angle (WCA). Biotextile hydrophilicity was measured via WCA, in which angles less than 90 degrees are indicative of hydrophilic surfaces, while greater than 90 degrees are characteristic of hydrophobic properties. Room temperature deionized water (10 uL) was deposited onto microbial cellulose surfaces, and contact angles were measured using a contact angle goniometer (Ramé-hart, Inc., Mountain Lakes, NJ, USA) with a fiber optic illuminator (Dolan-Jenner Industries, Inc., Woburn, MA, USA).

4.2.3 Mechanical properties. Mechanical properties were assessed by securing samples with custom clamps and mounting in a uniaxial tensile testing machine (Instron, Model 1321, Norwood, MA, USA), equipped with a 25 kN load cell. Biotextiles were maintained to have a gauge length of 2 inches and were tested to failure. Microbial cellulose elastic modulus, toughness, and ultimate tensile strength were determined from the stress-strain curve.

4.2.4 X-ray Diffraction. A 5-10 mm punch pressed into each of the various treated samples to create a series of small disks. The disks were placed on a standard glass slide. Diffractograms were collected using a Panalytical XPert3 Powder diffractometer with a 3 kW generator, fully ceramic Cu Long fine focus (LFF), X-ray tube, vertical goniometer (theta-theta) and a PIXcel 1d detector. The copper long fine focus lens produces a K- alpha of 1.5406 angstroms. Measurements were collected while scanning from 5 to 100 degrees with the following parameters: Fixed divergence slit: 1/2 degree, step size: 0.026 deg/step, scanning rate: 10.7 deg/min. A background was obtained by measuring the blank sample holder before taking measurements. A baseline correction was applied using Highscore XRD software.

The lattice spacing (d-spacing) was calculated using Bragg's equation:

$$\lambda = 2d_{hkl}*\sin\theta$$

where d_{hkl} is the lattice spacing of the crystallographic planes, θ is the corresponding Bragg angle, and λ is the X-ray wavelength (0.154 nm).

The Crystallinity Index (CI) was calculated using the XRD peak deconvolution method[21] using Igor-Pro software to separate amorphous and crystalline contributions to the diffraction spectrum using a curve-fitting process. For the curve fitting, Gaussian functions were used for deconvolution of XRD spectra into four crystalline peaks (101, 10$\bar{1}$, 021, and 200) and one amorphous peak centered at a 2θ value of ~21.5 degrees. CI is calculated from the ratio of the area of all crystalline peaks to the total area.

It is generally accepted that peak broadening is due to the amorphous cellulose, but crystallite size is an equally important issue for peak broadening and can affect accuracy of CI values obtained with the deconvolution method. However, uniformity in average crystallite size for as-fabricated MC and processed (LT, LTS, S) biotextiles, calculated from this method using the Scherrer formula, validate the accuracy of using this approach, and attributing differences in Bragg peak ratios to amorphous and crystalline contributions (see Table S1).

Crystallite Size was obtained by calculating the Scherrer width via the Scherrer equation:

$$d_{hkl}=k\lambda/(FWHM*\cos\theta)$$

where d_{hkl} is the size of the crystallite in nm, λ is the x-ray wavelength, is the FWHM of the peak, k is the Scherrer constant of 0.94 and θ is the diffraction angle (2θ is the corresponding peak position).

4.2.5 Thermal Analysis. A 45º Flame Test (ASTM D1230-94), which is a widely-accepted method for determining apparel textiles flammability, was used to measure: 1) Ease of textile ignition, and the 2) Duration of flame spreading. Biotextiles (1"x 6" in Figure 3 and Figure S2 and 1"x18" in Figure S3) were mounted and held in a custom apparatus at an 45º angle. A standardized flame was applied to one end of the biotextile at a 45º angle, using 14.1 oz. Map-Pro Cylinder by Bernzomatic, which uses liquid propane as a fuel source and has a flame temperature in air of 3,730° F/2054.4° C.

Charred biotextile surfaces were observed with SEM. Thermal properties and char formation of dried, pre-weighed microbial cellulose discs (diameter: 4.5 mm) were determined by a thermogravimetric analyzer (TGA 550, TA Instruments; New Castle, DE). TGA analysis was performed at a heating rate of 10ºC/min over the temperature range of 25ºC to 700ºC under flowing nitrogen (40 mL/min), in which final weights indicated the formation of char residue.

4.2.6 Chemical and elemental analysis. FTIR, XPS, and EDAX were performed to characterize microbial cellulose mechanical, hydrophilic, and thermal properties. FTIR (LUMOS II, Bruker, Billerica, MA, USA) spectra were recorded under attenuated total reflectance (ATR) mode in a spectral range of 4000-600 cm^{-1}. Each spectrum was collected using a total of 200 scans and a resolution of 4 cm^{-1}.

Cellulose chains contain both crystalline (ordered) and amorphous (unordered) regions. To determine the relative amount of crystallinity in materials, the Crystallinity Index (CI) can be determined by XRD, ^{13}C and FTIR. Determination of CI from FTIR has been found to be the easiest, however, these results only provide relative values because cellulose contains both crystalline and amorphous regions.

Crystallinity analysis of the biotextiles with FTIR data was performed using empirical formulas proposed by Nelson and O'Connor.[42] The first calculation is the Lateral Order Index (LOI: A_{1420}/A_{893}), also known as the empirical crystallinity index, relates to the overall degree of order in cellulose. The peak around 1420 cm^{-1} relates to the presence of crystalline regions, while the peak around 893 cm^{-1} is associated with amorphous regions. The second calculation is the Total Crystallinity Index (TCI: A_{1375}/A_{2900}) is also used to evaluate crystallinity. While the ratio between absorbances at 1429 cm^{-1} to 897 cm^{-1} is defined as the lateral order index (LOI) required to assess cellulose's overall degree of order, the ratio between 1372 cm^{-1} to 2900 cm^{-1} is defined as total crystallinity index (TCI), which is related to the degree of crystallinity in cellulose. The formulas used for these calculations are as follows:

$$\text{LOI} = \frac{A\,(1420)}{A(\,893)}$$

$$\text{TCI} = \frac{A\,(1375)}{A(\,2900)}$$

4.2.7 Determination of Hydrogen Bonding Environment Via FTIR

The relative absorbance (A) for the band at a specific wavelength (λ) attribute to the hydrogen bonds in the material is calculated using the C–H stretching band as an internal standard. The empirical formula is:

$$Ar_{\lambda} = \frac{A_{\lambda}}{A_{C-H}} = \frac{A_{897,\,1375,1430}}{A_{2920}}$$

The bands 2920 cm^{-1}, 1372 cm^{-1} and 1423 cm^{-1} are assigned to the C–H stretching in the methylene groups, aliphatic C–H stretching, and aromatic skeletal vibrations combined with C–H in plane deformations, respectively. According to the empirical formula, the absorbance ratio of the bands at 897 cm^{-1} (Ar_{897}), 1375 cm^{-1} (Ar_{1375}), and 1430 cm^{-1} (Ar_{1430}) to 2915 cm^{-1} correspond to the degree of hydrogen bonds destroyed; with decrease in ratio signifying an increase in hydrogen bonding strength.[30]

4.2.8 X-ray Photoelectron Spectroscopy (XPS). After samples were vacuum annealed at 75°C 24 hours, XPS was measured with PHI 5500, Chanhassen, MN, USA The spectra were recorded using a monochromatic Mg-Ka radiation X-ray source (1253.6 eV) and the analyzer pass energy was set to 25 eV. The sample chamber was set to 50 W operating at 15 kV voltage and a base pressure of 2 $x10^{8}$ torr. The XPS spectra were collected in the range from 0

to 1200 eV, with a resolution of 0.1-1.0 eV. A Shirley background subtracted was performed to remove the inelastic background of the carbon (C 1s), oxygen (O 1s), nitrogen (N 1s), and phosphorous (P 2p) electron core spectra and data was analyzed using commercial curve fitting software Igor64 (WaveMetrics, Portland, OR, USA). The binding energy scale was calibrated using the Au 4f 4/7 line of 10 nm thick gold, electron beam evaporated into 5 mm wide strips onto two parallel edges of the LT and MC samples, and confirmed against the C 1s binding energy for adventitious carbon on Au (285 eV) as well as published XPS data for microbial and plant cellulose. Based on these values, MC and LT XPS data were shifted -1.98 and -2.88 eV to higher binding energy, respectively. A smoothing factor of 10 was applied to the P 2p XPS data for ease of comparison (no smoothing was applied to C 1s or O 1s data). Further surface elemental characterization was assessed by an EDS system (Bruker XFlash 6, Billerica, MA, USA; 10 kV; 5 minutes; n=3) connected to a scanning electron microscope (Zeiss Sigma VP, Oberkochen, Germany). Biotextiles were sputter coated (Cressington 108, Watford, UK) with copper, and assessed for the presence of phosphorus.

4.3 Natural Dye Coloration. With the exception of indigo and logwood dyed biotextiles, natural dye matter was added with tea and sugar for coincident extraction of color and preparation of the cultivation media and strained before adding bacteria inoculum to the media- so that color could be directly incorporated into the nanofiber mesh during biosynthesis. Details oft he dye procedures are included in the Supporting Information.

4.4. Life cycle impact assessment (LCA). LCA analysis was performed using International Standards ISO 14040 and 14044. Manufacturing impacts were determined using Sustainable Minds® Life Cycle Assessment software (Cambridge, MA, USA) and the EcoInvent database (Zurich, Switzerland). The impact categories are based on the U.S. EPA's Tool for the Reduction and Assessment of Chemical and other Environmental Impacts (TRACI) life cycle impact assessment (LCIA) methodology. As defined by the software, ecological damage is comprised of acidification (kg SO_2 eq), ecotoxicity (CTUe), eutrophication (kg N eq), global warming (kg CO_2 eq), and ozone depletion (kg CFC^{-11} eq). Human health damage includes carcinogenics and non-carcinogenics (both in units of CTUh), respiratory effects (kg PM2.5 eq, fine particulates), and smog (kg (ground level) O_3 eq), while resource depletion exclusively refers to extraction of fossil fuels (MJ surplus). A complete description of the LCA scope, data sets and detailed comparison can be found in the Supporing Information.

4.5 Biodegradation Studies. Dry 20 mm x 20 mm samples (n=5) of as grown and lecithin tanned microbial cellulose were weighed and buried in pots containing soil, pH 6.9, with N, P, and K concentrations exceeding 4, 3, and 5 ounces per 100 square feet, respectively, as measured with a Luster Leaf Rapid Soil Analysis test (model 1601). After 60 days outdoors; with average high and low temperatures for the 60-day period were 14.2 and 3.2 C, respectively, samples were removed and weighed.

4.6 Statistical analysis. All quantitative values are reported as means ± standard deviation, with *n* equal to the number of replicates per group. Two-way analysis of variance (ANOVA) and the Tukey-Kramer post-hoc test was used for all pairwise comparisons, and significance was attained at $p<0.05$. Statistical analyses were performed with JMP-IN (4.0.4, SAS Institute, Inc., Cary, NC, USA).

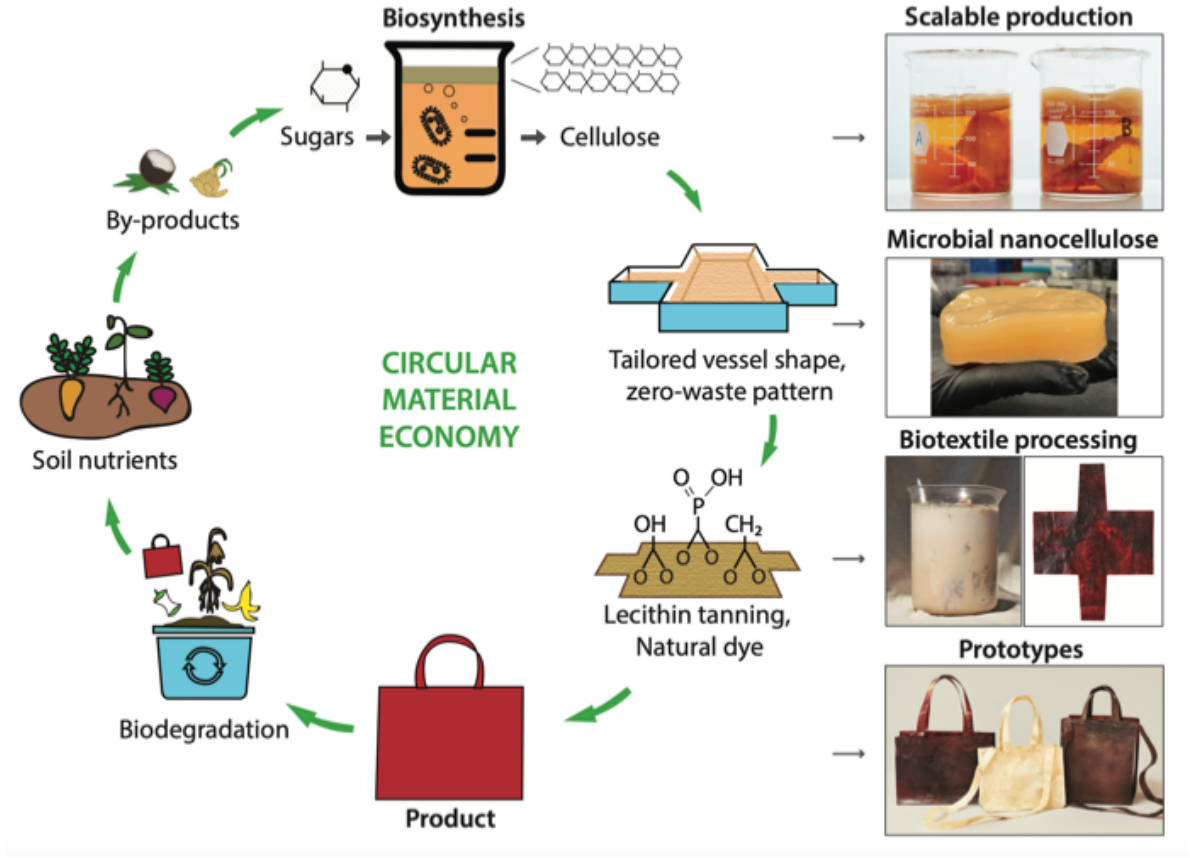

Figure 1. Potential of microbial biosynthesis and processing based in green chemistry to create minimal waste products with a closed loop life cycle (left). Right panel: Process photos for biosynthesis and processing of MC biotextiles for the schematic diagram on left, showing: scalable production of microbial nanocellulose from a variety of carbon sources, including fructose (beaker A) and sucrose (beaker B) and green chemistry processing--lecithin tanning and natural dye coloration--of biotextiles grown to the geometry of a bag pattern, to create low impact, minimal waste products, such as our bioleather bag prototypes, that meet design criteria of performance and biodegradability for a regenerative, circular materials economy.

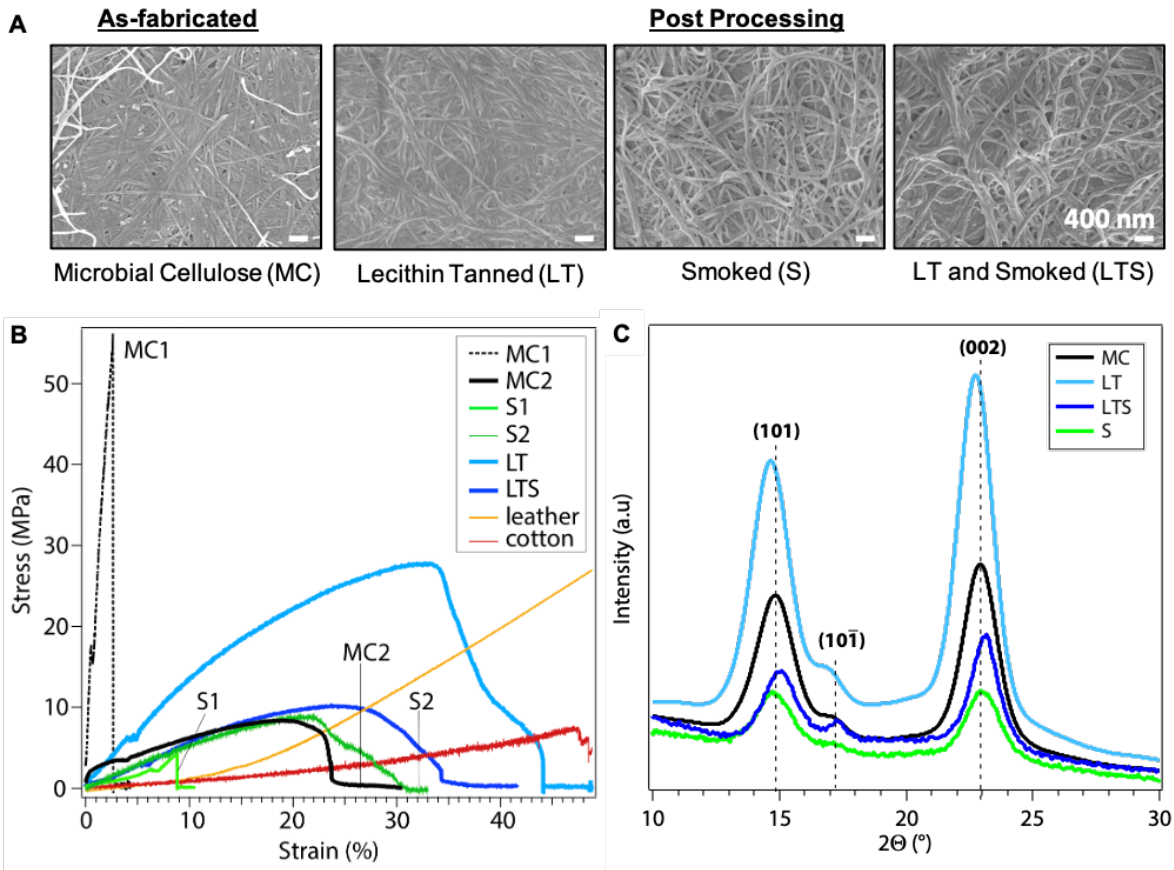

Figure 2. Physiochemical Characterization of Microbial Cellulose Biotextiles. (A) SEM micrographs; **(B)** tensile properties; and **(C)** XRD data; for as grown microbial cellulose (MC) and microbial treated by lecithin (LT) and/or smoke tanning (LTS, S). MC1 and MC2 and S1 and S2 were produced from the same biosynthesis and processing conditions; the variation reflects the influence of MC hygroscopicity on mechanical properties which is overcome with lecithin tanning (LT).

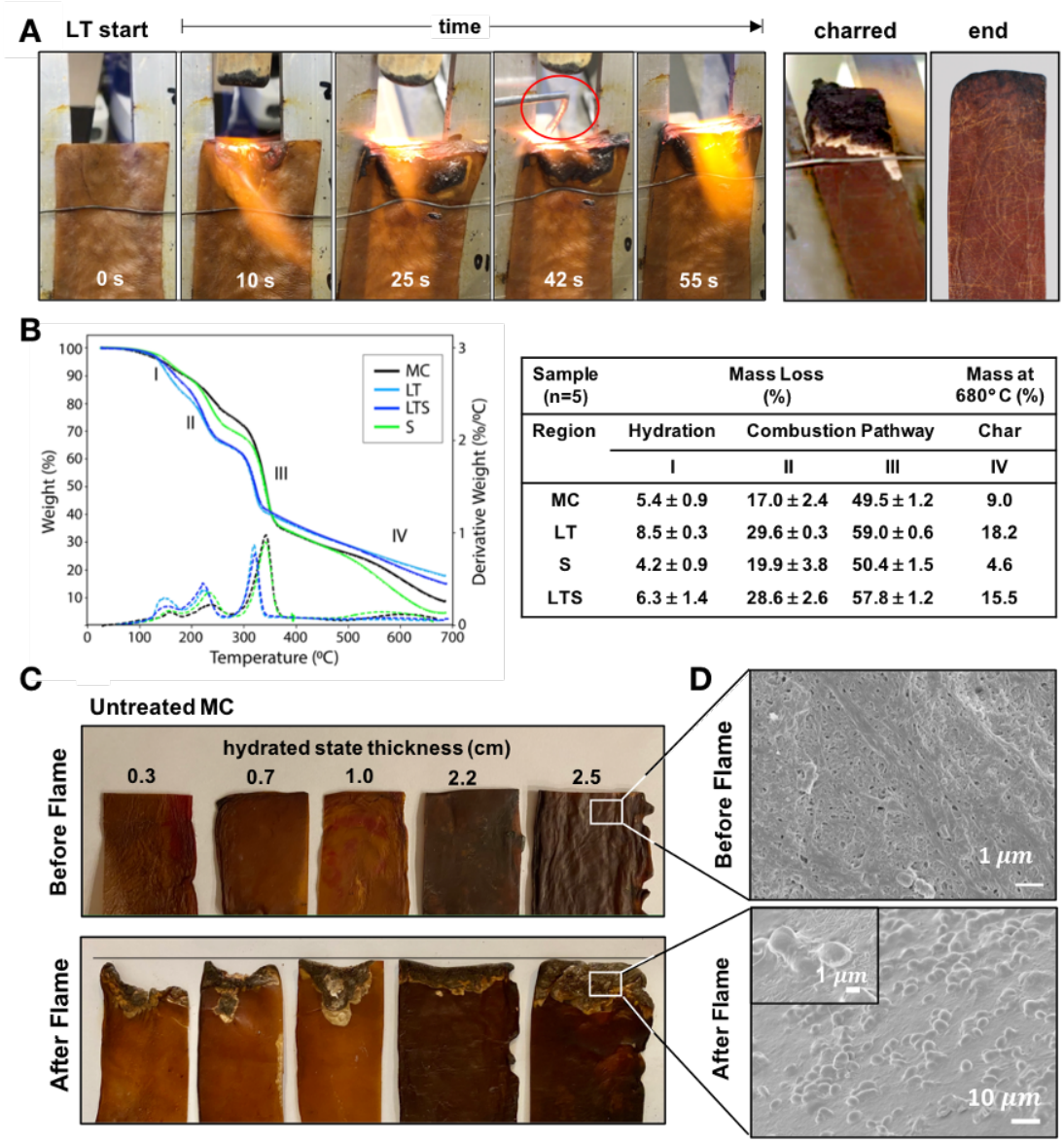

Sample (n=5)	Mass Loss (%)			Mass at 680° C (%)
Region	Hydration	Combustion Pathway		Char
	I	II	III	IV
MC	5.4 ± 0.9	17.0 ± 2.4	49.5 ± 1.2	9.0
LT	8.5 ± 0.3	29.6 ± 0.3	59.0 ± 0.6	18.2
S	4.2 ± 0.9	19.9 ± 3.8	50.4 ± 1.5	4.6
LTS	6.3 ± 1.4	28.6 ± 2.6	57.8 ± 1.2	15.5

Figure 3. Flame Retardance of Microbial Cellulose Biotextiles. (A) Under a 2054° C flame, lecithin tanned microbial cellulose (LT) does not ignite and deflects the flame from the surface, while an aluminum brazing rod introduced at 39 seconds promptly melts under the flame. After repeated exposure until char formation is observed (charred), LT biotextiles remain intact under the surface ash (end). (**B**) Thermal decomposition analysis (TGA) curves (left) and data (right) of as-fabricated (MC) and treated (LT, S, LTS) biotextiles under nitrogen atmosphere shows the phospholipid treatment directs the combustion chemistry toward ash formation over the glucosan formation to promote flame retardance. (**C**)The nanofiber morphology and layered microstructure of as-fabricated MC biosynthesized to sufficient thickness (2.5 cm in hydrated state) also demonstrates flame retardance, evidence by resistance to material lost to combustion. (**D**) SEM micrograph showing surface morphology before (top) and in charred region after (bottom) flame testing; the torched region of the latter shows a morphology typical of a flame-retardant material.

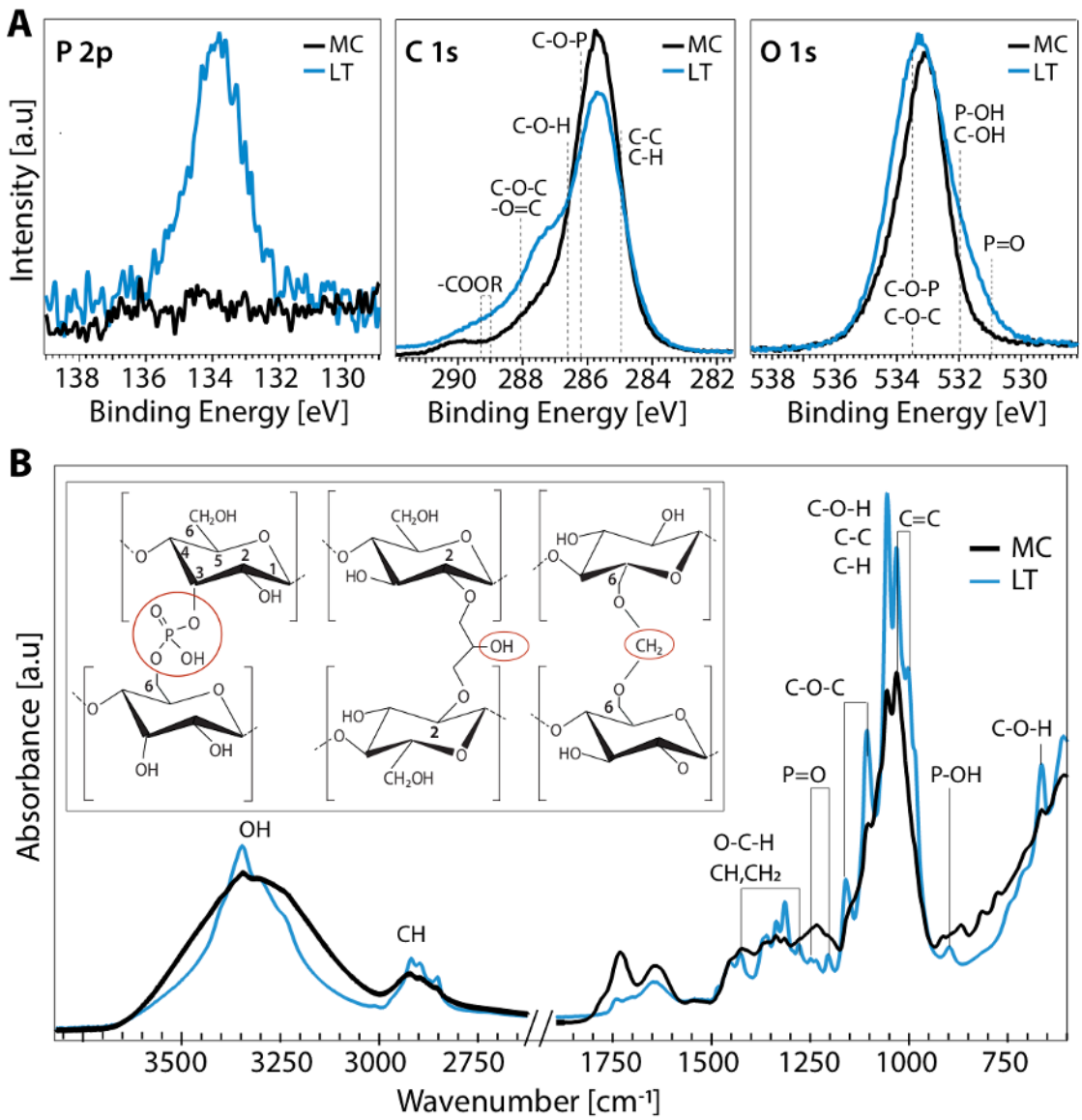

Figure 4. Molecular-Level Chemical Analysis. A) X-ray photoelectron spectroscopy (XPS) and **(B)** Fourier Transform Infrared (FTIR) spectra of microbial cellulose textiles before (MC) and after lecithin tanning (LT). **Inset**: schematic depiction of proposed cross-linking mechanism with phosphate, methylene and carboxyl group bridges (left to right) for LT.

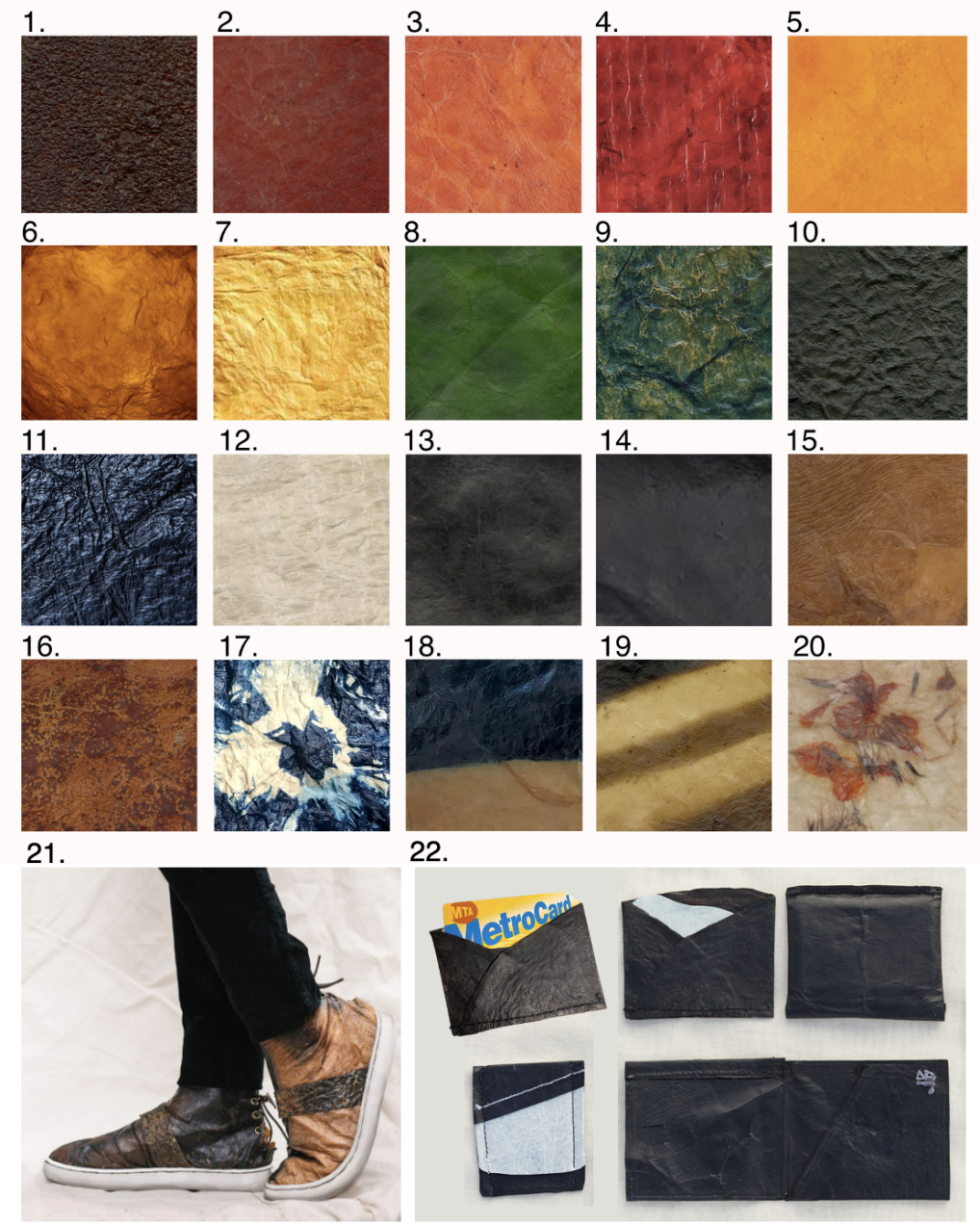

Figure 5. **Natural Dye Color Palette on Microbial Biotextiles**. (**1-3**) madder root; (**4**) cochineal, (**5**) marigold; (**6**) turmeric; (**7**) onion skins; (**8**) chlorophyll; (**9**); indigo after one (**9**), three (**10**) and six (**11**) dips; (**12**) brown color removed by 0.5 M NaOH soak; black created by chemical interaction of tannic acid from black tea with iron acetate, extracted from discarded nails (**13**); and myrobalan overdyed with logwood and dipped in iron acetate (**14**); (**15-16**) as-fabricated MC treated with texture created by application of soy wax heated to 80C. Control of color modulation through: Shibori/Adire folding techniques (**17**); and partial submergence of biotextile in indigo vat (**18**). (**19**) Dark stripes obtained by chemical interaction of iron acetate and tannic acid on as-fabricated MC; and (20) marigold flowers embedded between MC pellicle layers before drying, adapted from Japanese Hapa Zome techniques, showing design opportunities such as no sew seams offered by the layered structure of the moldable biotextile. Design prototypes, including (**21**) sneakers in natural color and an upcycled rubber sole; and (**22**) bioleather wallets with natural black as in (**14**) before lecithin tanning and drying and with white as in (**12**). See Methods for details.

Figure 6. **Life Cycle Impact Assessment (LCA) of Microbial Cellulose Biotextiles.** Cradle to gate LCA for the industrial manufacture of 1 m^2 of conventional textile, including cow leather, synthetic leather (PU textile (polyurethane-coated polyester), and woven cotton, compared with laboratory-scale biofabrication (microbial fermentation and lecithin processing) of MC ($biotextile_{LAB}$), and biotextiles processed (purified and lecithin tanned) from MC obtained as SCOBY by-product of commercial kombucha beverage production ($biotextile_{BP}$). **(A)** Comparison of environmental impact categories for the different textiles; Human toxicity corresponds to impacts from carcinogenics and hormonally active agents (HAA), while ecological damage includes acidification, ecotoxicity, eutrophication, global warming and ozone depletion **(B)** Contributions to total impacts from different impacts categories (legend) and source of largest impacts.

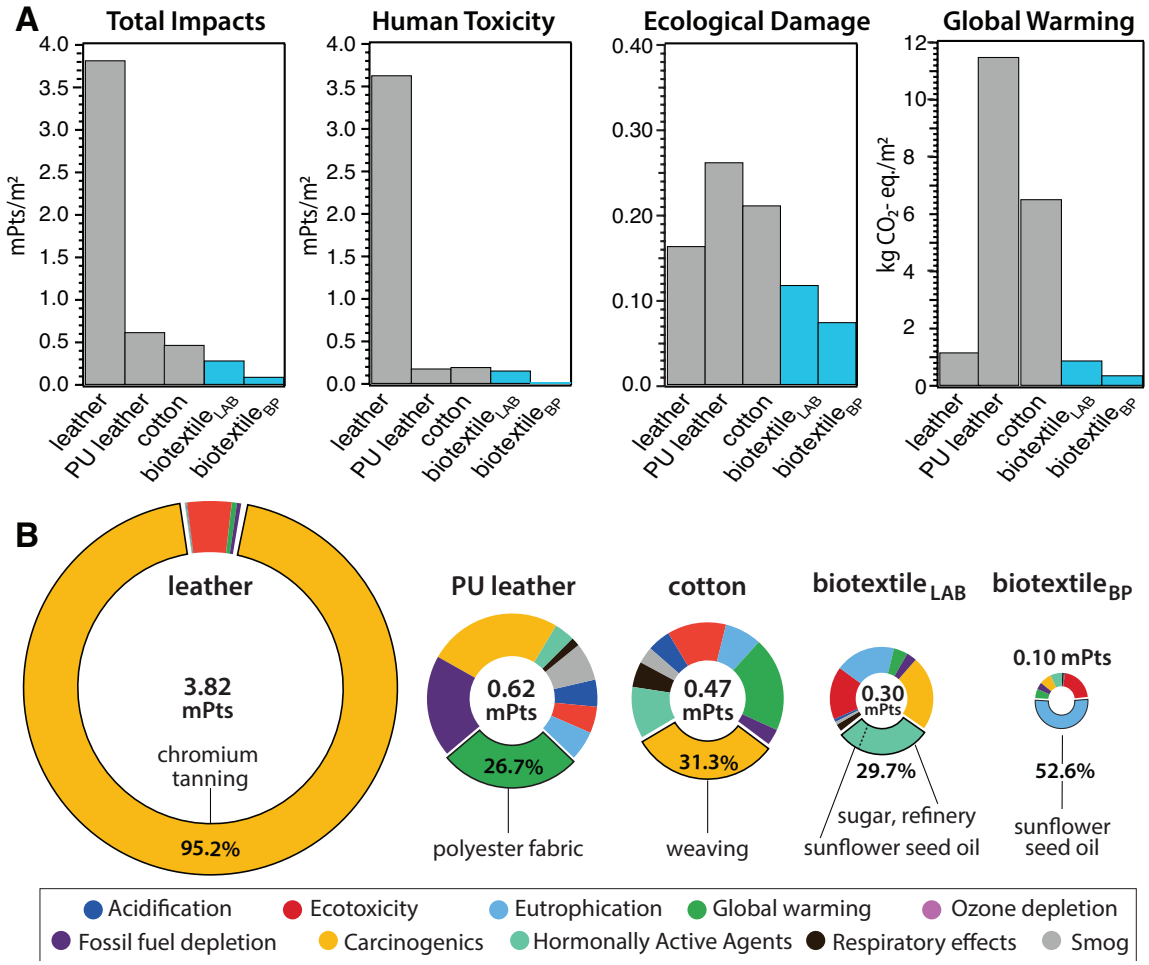

Table 1. Physiochemical properties of as-fabricated and treated biotextiles compared to cotton and leather. Mechanical properties, including Young's Modulus, Toughness and Max Strength (n=4), crystallinity index obtained from x-ray diffraction, fiber diameter (n=100), and water contact angle (WCA, n=5)) for as-fabricated (MC) and processed (LT, S, LTS) for samples shown in Fig. 2. *Fiber diameter for leather based on published data *(41)*. ^ indicates significance between groups (α = 0.05, n=5). All quantitative values are reported as means ± standard deviation, with n equal to the number of replicates per group, with significance was attained at $p<0.05$.

	Young's Modulus (MPa) n=4	Toughness (MPa) n=4	Max. Strength (MPa) n=4	Fiber Diameter (nm) n=100	Crystallinity Index (%) n=5	WCA (°) n=5
MC1	210.9 ± 58.6	2.5 ± 0.6	17.4 ± 4.6	71.0 ± 19.0	84.12 ± 0.03	61.9 ± 12.4
MC2	58.30 ± 35.7	2.44 ± 1.4	12.0 ± 5.8			
LT	196.4 ± 65.4	7.2 ± 2.3	27.9 ± 1.8	69.4 ± 16.8	87.19 ± 0.07	46.5 ± 10.9
LTS	89.8 ± 45.2	2.2 ± 0.3	11.1 ± 1.5	76.5 ± 16.2	77.00 ± 0.04	46.1 ± 6.2
S1	38.9 ± 19.1	0.1 ± 0.05	3.4 ± 1.5	56.6 ± 14.7	67.51 ± 0.04	58.4 ± 7.0
S2	24.0 ± 3.3	1.5 ± 1.0	5.5 ± 2.8			
cotton	19.7	2.6	8.0	1.27 ± 0.3 E04	-	-
leather	75.9	5.4	28.4	10 E04*	-	-

Supporting Information

Supporting Information is available from the Wiley Online Library or from the author.

Funding

National Science Foundation, MRSEC program through Columbia in the Center for Precision Assembly of Superstratic and Superatomic Solids, grant DMR-1420634 (TNS, RA, Y-TC, CTJ, SE, DA, STR).

National Institutes of Health, grant NIH-NIAMS 1R01-AR07352901 (RA, Y-TC, HHL).

DoD CDMRP award, grant W81XWH- 15-1-0685 (RA, Y-TC, HHL).

Acknowledgements

We thank OM Champagne Tea (Mount Kisco, NY) for donations of microbial nanocellulose, produced as a fermentation by-product of commercial kombucha beverage production. The bioleather sneakers shown in the ToC figure were created in collaboration with Dao-Yi Chow and Maxwell Osbourne of Public School, for the OnexOne Conscious Design Initiative.

References

[1] M. A. Altieri, Ecological impacts of industrial agriculture and the possibilities for truly sustainable farming. *Monthly Review,* **1998**, 50, 3.

[2] S. S. Muthu, *Assessing the Environmental Impact of Textiles and the Clothing Supply Chain*, (Woodhead Publishing, 2nd Edition) **2020**.

[3] P. Chrobot, M. Faist, L. Gustavus, A. Martin, A. Stamm, R. Zah, M. Zollinger, "Measuring fashion: Insights from the environmental impact of the global apparel and footwear industries study" (Quantis, **2018**; https://quantis-intl.com/wp-content/uploads/2018/03/measuringfashion_globalimpactstudy_full-report_quantis_cwf_2018a.pdf).

[4] World Bank, "The Bangladesh responsible sourcing initiative: A new model for green growth?" (World Bank, **2014**;https://openknowledge.worldbank.org/handle/10986/20764).

[5] Institution of Mechanical Engineers, "Engineering out of fashion waste" (Institution of Mechanical Engineers, **2018**; https://www.imeche.org/policy-and-press/reports/detail/engineering-out-fashion-waste).

[6] Ellen MacArthur Foundation, "A new textiles economy: redesigning fashion's future" (Ellen MacCarthur Foundation Report, **2017**).

[7] E. Goldman, M.J. Weisse, N. Harris, and M. Schneider, "Estimating the Role of Seven Commodities in Agriculture-Linked Deforestation: Oil Palm, Soy, Cattle, Wood Fiber, Cocoa, Cofee, and Rubber." Technical Note. Washington, DC: World Resources Institute, **2020**. Available online at: wri.org/publication/estimating-the-role-of-sevencommodities-in-agriculture-linked-deforestation

[8] G. L. Tadesse, T. K. Guya, Impacts of tannery effluent on environments and human health. *Environ.* **2017**, 7, 3.

[9] Y. Deng, Y. Zhang, B. Lemos, H. Ren, Tissue accumulation of microplastics in mice and biomarker responses suggest widespread health risks of exposure. *Sci Rep*. **2017**, 7, 46687.

[10] A. Ragusa, A. Svelato, C. Santacroce, P. Catalano, V. Notarstefano, O. Carnevali, F. Papa, M. C. A. Rongioletti, F. Baiocco, S. Draghi, E. D'Amore, D. Rinaldo, M. Matta, E. Giorgini, Plasticenta: First evidence of microplastics in human placenta. *Environ. Int.* **2021**, 146, 106274.

[11] J. Hildebrandt, D. Thrän, A. Bezama, The circularity of potential bio-textile production routes: Comparing life cycle impacts of bio-based materials used within the manufacturing of selected leather substitutes, *J. Clean. Prod*. **2021**, 287, 125470.

[12] M. Gama, P. Gatenholm, D. Klemm, Ed., *Bacterial NanoCellulose: A Sophisticated Multifunctional Material* (CRC Press, **2012**).

[13] K.Y. Lee, G. Buldum, A. Mantalaris, A. Bismarck, More than meets the eye in bacterial cellulose: biosynthesis, bioprocessing, and applications. *Macromol. Biosci.* **2014**, 14, 10–32.

[14] G. Chen, G. Wu, L. Chen, W. Wang, F. F. Hong, L. J. Jönsson, Comparison of productivity and quality of bacterial nanocellulose synthesized using culture media based on seven sugars from biomass. *Microb. Biotechnol.* **2019**, 12, 677–687

[15] Q. Li, S. McGinnis, C. Sydnor, A. Wong, S. Renneckar, Nanocellulose life cycle assessment. *ACS Sustainable Chem. Eng.***2013**, 1, 919−928

[16] Í. Donini, D. De Salvi, F. Fukumoto, W. Lustri, H. Barud, R. Marchetto, Y. Messaddeq, S. Ribeiro, Biosynthesis and recent advances in production of bacterial cellulose. *Ecl. Quím*. **2010**, 35, 165-178.

[17] K. Kamiński, M. Jarosz, J. Grudzień, J. Pawlik, F. Zastawnik, P. Pandyra, A. M. Kołodziejczyk, Hydrogel bacterial cellulose: a path to improved materials for new eco-friendly textiles. *Cellulose.* **2020**, 27, 5353–5365.

[18] B. A. Howell, S. T. Lazar, Biobased Plasticizers from glycerol/adipic acid hyperbranched poly(ester)s, *Ind. Eng. Chem. Res.* **2019**, 58, 37, 17227–17234.

[19] A. G. Püntenera, S. Moss, Ötzi, the Iceman and his leather clothes. *Chimia.* **2010**, 64, 315–320.

[20] C. L. Heth, "The Skin They Were In: Leather and Tanning in Antiquity" in *Chemical Technology in Antiquity* (ACS Symposium Series **1211**, 2015), pp. 181-196.

[21] S. Park, J.O. Baker, M.E. Himmel, P.A. Parilla, D. K. Johnson, Cellulose crystallinity index: measurement techniques and their impact on interpreting cellulase performance. *Biotechnol. Biofuels*. **2010**, 3, 10.

[22] S. Zhang, S.N. Li, Q. Wu, Q. Li, J. Huang, W. Li, W. Zhang, S. Wang, Phosphorus containing group and lignin toward intrinsically flame-retardant cellulose nanofibril-based film with enhanced mechanical properties. *Compos. B. Eng*. **2021**, 212, 108699.

[23] C.M. Butt, J. Congleton, K. Hoffman, M. Fang, H. M. Stapleton, Metabolites of organophosphate flame retardants and 2-Ethylhexyl tetrabromobenzoate in urine from paired mothers and toddlers. *Environ. Sci. Technol*. **2014**, 48, 10432–8.

[24] G. Montaudo, E. Scamporrino, D. Vitalini, The effect of ammonium polyphosphate on the mechanism of thermal degradation of polyureas. *J. Polym. Sci., Polym. Chem. Ed.* **1983**, 21, 336.

[25] W. Wang, Y. Kan, H. Pan, Y. Pan, B. Li, K.M. Liew, Y. Hu, Phosphorylated cellulose applied for the exfoliation of LDH: An advanced reinforcement for polyvinyl alcohol. *Compos. Part A Appl. Sci. Manuf.* **2017**, 94, 170–177

[26] E.H. Ablouh, F. Brouillette, M. Taourirte, H. Sehaqui, M. El. Achaby, A. Belfkira, A highly efficient chemical approach to producing green phosphorylated cellulosic

macromolecules. *RSC Adv.* **2021**, 11, 24206-24216.

[27] M. Ghanadpour, B. Wicklein, F. Carosio, L. Wågberg, All-natural and highly flame-resistant freeze-cast foams based on phosphorylated cellulose nanofibrils. *Nanoscale* **2018**, 10, 4085-4095.

[28] D. M. Suflet, G. C. Chitanu, V. I. Popa, Phosphorylation of polysaccharides: New results on synthesis and characterisation of phosphorylated cellulose. *React. Funct. Polym.* **2006**, 66, 11, 1240-1249.

[29] N. Zhu, F.Z. Cui, K. Hu, L. Zhu, Biomedical modification of poly(L-lactide) by blending with lecithin, *J. Biomed. Mater. Res*. **2007**, 82A, 455-461.

[30] M. Fan, D. Dai, B. Huang, "Fourier transform infrared spectroscopy for natural fibres" in *Fourier transform-materials analysis* (Dr Salih Salih (Ed.), **2012**), pp. 45-68.

[31] A. Hebeish, J. T. Guthrie, *The Chemistry and Technology of Cellulose Copolymers: Polymers – Properties and Applications 4* (Springer-Verlag, **1981**).

[32] H. Guo, M. He, R. Huang, W. Qi, W. Guo, R. Su, Z. He, Changes in the supramolecular structures of cellulose after hydrolysis studied by terahertz spectroscopy and other methods. *RSC. Adv*. **2014**, 4, 57945

[33] M. Ryberg, M. Vieira, M. Zgola, J. Bare, R. Rosenbaum, Updated US and Canadian normalization factors for TRACI 2.1. *Clean Techn. Environ. Policy.* **2014**, 16, 329–339.

[34] T.P. Gloria, B.C. Lippiatt, J. Cooper, Life cycle impact assessment weights to support environmentally preferable purchasing in the United States. Environ. Sci. Technol**.** **2007**, 41, 21, 7551–7557.

[35] Swanton, John R. *"Indians of the Southeastern United States"*. Bureau of American Ethnology, Bulletin 137. Washington: Government Printing Office, **1946**.

[36] B. V. Mohite, S. V. Patil, A Novel, Biomaterial: Bacterial Cellulose and its New Era Applications. *Biotech. Appl. Bioc.* **2014**, 61, 101-110.

[37] A. Vazquez, M.L. Foresti, P. Cerrutti, *et al.,* Bacterial Cellulose from Simple and Low Cost Production Media by *Gluconacetobacter xylinus*. *J Polym Environ* **2013**, 21, 545–554.

[38] S.J. Kraham, "Environmental Impacts of Industrial Livestock Production" in *International Farm Animal, Wildlife and Food Safety Law*, G. Steier, K. Patel, Eds. (Springer, Cham. **2017**) pp 3-40.

[39] K. B. Murugesh, M. Selvadass, Life cycle assessment for the dyeing and finishing process of organic cotton knitted fabrics, *JTATM*. **2013**, 8, 2.

[40] N. Illy, M. Fache, R. Ménard, C. Negrell, S. Caillolc, G. David, Phosphorylation of bio-based compounds: the state of the art. *Polym. Chem.* **2015**, 6, 6257-6291.

[41] X. Li, Y. Wang, J. Li, B. Shi, Effect of Sodium Chloride on Structure of Collagen Fiber Network in Pickling and Tanning. *JALCA* **2016**, 111, 6, 203-237.

[42] M.L. Nelson, R.T. O'Connor, Relation of certain infrared bands to cellulose crystallinity and crystal lattice type. Part II. A new infrared ratio for estimation of crystallinity in celluloses I and II. *J. App. Polym. Sci*. **1964**, 8, 3, 1325-1341.

ToC

Microbial biosynthesis and bioprocessing, inspired by indigenous textile processes, are used to engineer high-performance, microbial biotextiles which mitigate the climate and toxicity impacts of conventional textiles. Biotextiles with superior mechanical and flame-retardant properties and a sustainable circular life cycle are demonstrated, including the plant- and mineral dyed bioleather sneakers shown.

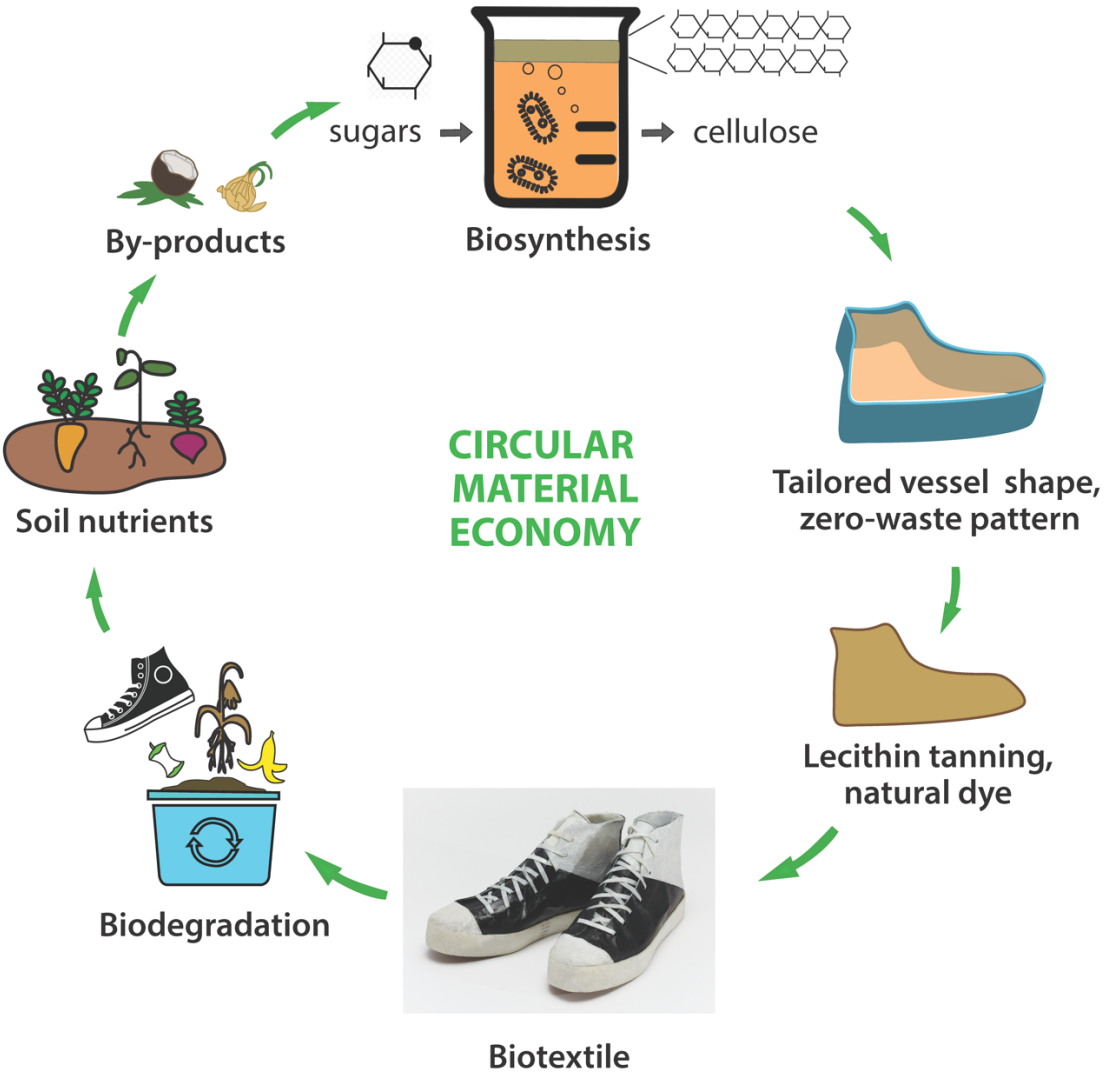

Supporting Information

Advanced Functional Biotextiles for a Circular Material Economy

Theanne N. Schiros[1,2]†, Romare Antrobus[3]†, Delfina Farias[1], Yueh-Ting Chui, Christian Joseph[2], Shanece Esdaille[2], Gwen Karen Sanchiricco[1], Grace Miquelon[1], Dong An[4], Sebastian T. Russell[4], Adrian Chitu[5], Susanne Goetz[6], Anne Marika Verploegh Chassé[7], Colin Nuckolls, [8] Sanat K. Kumar[4], Helen H. Lu[2]**

Affiliations:

[1]Department of Science and Mathematics, Fashion Institute of Technology; New York, NY 10001.

[2]Materials Research Science and Engineering Center, Columbia University; New York, NY 10027.

[3]Department of Biomedical Engineering, Columbia University; New York, NY 10027.

[4]Department of Chemical Engineering, Columbia University; New York, NY 10027.

[5]Materials Science and Engineering, Columbia University; New York, NY 10027.

[6] Surface/Textile Design, Fashion Institute of Technology; New York, NY 10001.

[7] Footwear and Accessories Design, Fashion Institute of Technology; New York, NY 10001.

†These authors contributed equally to this work.
Correspondence to: ts2526@columbia.edu and hhlu@columbia.edu

This PDF file includes:

Materials and Methods
Supporting Information
Figs. S1 to S7
Tables S1 to S9
Captions for Movie S1 and S2

Other Supporting Information for this manuscript include the following:

Movie s1
Movie s2

Materials and Methods

Natural (plant, insect and mineral) dyeing of microbial cellulose biotextiles

To reduce the water and energy demands of traditional dip dye methods, natural dye matter was added with tea and sugar for coincident extraction of color and preparation of the cultivation media and strained before adding bacteria inoculum to the media- so that color could be directly incorporated into the nanofiber mesh during biosynthesis. The tannins in the tea serve to mordant the cellulose fibers, to improve color retention, saturation and colorfastness. Cultivation vessels were prepared with 5.3% w/v sugar, 4% w/v tea, 10% v/v starter culture and natural dye matter.

Dye procedures are as follows. A madder root 9.75% w/v post synthesis dye bath was used for **Figure 5.1**. The following dye stuff was incorporated directly into the culture media so that color was incorporated into the microbial cellulose matrix *during* biosynthesis: 10% w/v madder using black tea (**Figure 5.2)** and green tea **(Figure 5.3**) as the nitrogen source in the fermentation media (the swatch shown in Figure 5.3 was dried from a pellicle grown to half the hydrated state thickness of that in **Figure 5.3**); 7.5% w/v cochineal (**Figure 5.4**); 5% w/v; marigold extract (**Figure 5.5**); turmeric 20% w/v; (**Figure 5.6**); 7.5% v/v liquid chlorophyll (**Figure 5.8**). The swatch in **Figure 5.7** was colored using yellow onion skins 3% w/v as a post processing dye bath, after color was removed using the process described below for the white swatch shown in **Figure 5.12**. Onion skins were obtained as food by-product and chlorophyll was obtained from Horbåach, Melville, NY. Marigold flowers were harvested locally at the end of season bloom and embedded between layers of the hydrated MC biofilm and hammered flat using the ancient Japanese textile art technique of hapa-zome, before the biotextile was left to dry flat on a flat polypropylene tray under ambient conditions (**Figure 5.20**). All other dye stuff was obtained from Botanical Colors, Seattle, Washington.

For red shown in main text **Figure 5.4** and **Figure 1**, 10 grams of cochineal were ground to a fine powder, placed in a cotton muslin pouch and tied with cotton string, and immersed in 250 ml distilled water and brought to 100 ºC for 15 minutes. The heat was turned off, allowed to sit for 15 minutes, after which the process of adding water and bringing to a boil was repeated 3 times. On the last step the tea and sugar for the culture media were added, after which the

cochineal pouch was removed, the additional water for the culture media was added, cooling the media to a temperature suitable to add the inoculum (10% v/v). Other colors were extracted in one liter of water held at 85ºC to 45-1 hour, and either added directly to the biosynthesis media after cooling or used as a post-processing dip dye bath, except for chlorophyll, which was added at room temperature with the inoculum to the media.

Post synthesis dip dyeing in room temperature organic indigo vats, produced from combining 5 g organic indigo powder, 10 g calcium hydroxide and 15 g fructose in 15 liters of water were used to create greens (**Figure 5.9**) and blues (**Figure 5.10-5.11, 5.17**). White biotextiles were achieved by immersion of hydrated MC in 0.5 M NaOH at room temperature for 12 hours, followed by rinsing in distilled water until a neutral pH was reached (**Figure 5.12**). Black coloration on the biotextile shown in **Figure 5.13** was achieved by chemical reaction of tannic acid and Fe acetate. Samples were immersed in a 3% w/v tannic acid solution, obtained from Botanical Colors, followed by a dip in aqueous Fe acetate mordant, prepared by soaking 100 grams of nails in 2 liters of 2.5% v/v acetic acid for two weeks. Black biotextiles shown in **Figure 5.14** and used for the prototypes shown in **Figure 5.22** were created in a post-processing overdye procedure as follows: 10% w/v myrobalan bath, brought up to 55ºC before MC biotextiles were added, and heating was continued to a high simmer (~83ºC) and held for one hour. MC biotextiles were removed from the myrobalan bath, rinsed twice, and left to cool before being added to a 15% w/v logwood extract bath at 33ºC. The logwood bath was held at this temperature for 30 minutes, after which the temperature was gradually increased to 80ºC) for 45 minutes. MC biotextiles were rotated gently throughout the post-synthesis dye process, and left to cool in the dye bath, then rinsed twice before being dipped in Fe acetate for 10 seconds, and rinsed three times.

All post-processing dye baths were saved for repeated use (usually three more dye processes) until color diminished. After harvesting colored MC pellicles, all in situ dye baths were resupplied with cultivation media nutrients for at least 3 harvests.

Variation in surface texture shown in **Figure 5.1, 5.15 and 5.16** was achieved using soy wax heated to ~83ºC, spread across the biotextile surface with a brush, and pressed against an aluminum foil-covered hot plate for 10 seconds. Other surface variation was introduced by drying with tension (edges of biotextile clipped to a flat surface, **Figure 5.13-5.14; 5.18-5.19**) or without tension, as shown in **Figure 5.7-5.11**, or dried on a screen (**Figure 5.4**).

Life cycle impact assessment (LCA)

LCA analysis is a quantitative technique to assess the environmental and human health impacts associated with all the stages of a product's life, which is from raw material extraction through materials processing, manufacture, distribution, and use as specified in ISO 14040 standards, including International Organization for Standardization (ISO). Environmental Management - Life-Cycle Assessment-Principles and Framework, International Standard 14040; ISO: Geneva, Switzerland, 2006. International Organization for Standardization (ISO). Environmental Management - Life Cycle Assessment - Requirements and Guidelines, International Standard 14044; ISO: Geneva, Switzerland, 2006.[1] Manufacturing impacts were determined using Sustainable Minds® Life Cycle Assessment software (Cambridge, MA, USA) and the EcoInvent database (Zurich, Switzerland). The impact categories are based on the U.S. EPA's Tool for the Reduction and Assessment of Chemical and other Environmental Impacts (TRACI) life cycle impact assessment (LCIA) methodology. As defined by the software, ecological damage is comprised of acidification (kg SO_2 eq), ecotoxicity (CTUe), eutrophication (kg N eq), global warming (kg CO_2 eq), and ozone depletion (kg CFC^{-11} eq). Human health damage includes carcinogenics and non-carcinogenics (both in units of CTUh), respiratory effects (kg PM2.5 eq, fine particulates), and smog (kg (ground level) O_3 eq), while resource depletion exclusively refers to extraction of fossil fuels (MJ surplus).

Impacts were calculated in a cradle-to-gate LCA comparing the impacts of biofabrication microbial biotextiles using the methods described above with the manufacturing impacts of conventional textiles, including chrome tanned leather, synthetic leather (polyurethane (PU)-coated textile), and woven cotton. The functional unit is $1m^2$ of textile. For direct comparison, impacts were calculated from weighted impact categories, in milliPoints(mPts)/m^2) of textile, utilizing normalization and weighting factors shown in **Table S3**.[2] A point (1000 mPts) represents the average person's annual environmental load (*i.e.* entire production/consumption activities in the economy) in the United States.[3] Normalization factors were calculated using characterization factors from the TRACI 2.1 LCIA model, and toxicity-based categories use characterization factors calculated with USEtox. Weighting factors represent degree of immediate concern or degree to which remedial actions associated with the impact are underway, and provide a practical method to link quantitative results of LCA with environmental performance of competing products and assist environmentally preferable

design, manufacture, and purchasing.[4] A cradle-to-gate partial product life cycle was performed from resource extraction (cradle) to the factory gate which includes raw material and manufacturing impacts, with distribution, consumer use and disposal omitted; such assessments are often used as the basis for environmental product declarations (EPD).

LCA Rationale: Market data of the leather and synthetic leather goods industry.

Both synthetic and animal leather are frequently utilized within the apparel, automotive, and furnishing industries. According to Grand View Research.[5] The global synthetic leather market size was valued at 29.3 billion USD in 2019 and was expected to increase to 30.3 billion USD for 2020. It is also estimated that the market size volume in 2020 accounted for 15,585.6 million meters. The market size value of animal leather is estimated to have been over USD 80 billion in 2019.[6] As reported by Grand View Research, the textile market size value in 2020 is USD 1,000.30 billion. Subsequently, cotton was anticipated to be the largest raw material segment, accounting for a market share of 39.5% in 2019.[7]

Synthetic Leather

Synthetic leather (polymer coated textile) can be produced with a variety of synthetic polymers, including polyvinyl chloride (PVC), polyvinylidene chloride (PVDC), polyurethane (PU), and different base fibers (cotton, polyester or cotton/synthetic blends), and coating techniques. Each one of these variables affects the ecological impact of synthetic leather. The variation chosen for this LCA is PU-coated polyester made by the company Kuraray, specifically their product called Clarino Crust. According to market research, this enterprise is one of the main manufacturers of synthetic leather, and the material inventory created in the EcoInvent database are based on the manufacturing processes used by Kuraray.[8] According to Kuraray's Clarino Crust technical sheet, the weight of the textile is 0.66± 0.02 kg/m^2 and contains 90% of polyester (PET)- 0.594 kg - and 10% polyurethane (PU) -0.066 kg. The only information taken from the Clarino Crust technical sheet is the weight and the percentage -of PU and PET- utilized.[9]

The polyester was modeled with average data for dyed, manufactured polyester fabric for apparel in the EcoInvent database within the Sustainable Minds software. The PU coating system of materils was built from the average values material inputs for the urethane composition of use in synthetic leather.[10] In particular, t*he urethane composition is the dry method urethane composition.* In parts by weight, the dry method urethane composition

includes lower components: Solvent type polyurethane resin 80-100 parts (average 90 parts), acid additive 1-2 parts (average 1.5 parts), dimethylformamide 5-30 parts (average 17.5 parts) and ethyl acetate 10- 20 parts (average 15 parts). The inventory included 59.4 g epoxy (PU) resin (CAS number: 025928-94-3), 9.9 g ethyl acetate (CAS number: 000123-86-4), 1 g citric acid from fermentation (1 g), 11.55 g N,N-diemthylformamide (CAS number: 000068-12-2), and polyester fabric (594 g). Electricity, water use and transportation were not included.

For comparison, we also modeled the material inputs for the PU coating using the data set for PU flexible foam included in the EcoInvent database within Sustainable Minds, CAS number: 009009-54-5, provided by Kuraray, which includes the transport of the monomers, the production (energy, air emissions) of the PU foam, and using average values of transport and infrastructure, for the typical composition for European conditions and present technology used in Europe. The two models for the PU coating yielded similar impacts values and distributions across categories. The process of foaming by expanding plastic involves converting the plastic foam into an emulsion and then coating the base fabric.[11] The process data set included the auxiliaries and energy demand for the conversion process of plastics and the converted mass of plastic was not included in the dataset. The complete system of materials used to model the manufacturing of PU-coated polyester, obtained from the Ecoinvent database, is shown in **Tables S4** and **S5.**

<u>Cow leather</u>

The functional unit is $1m^2$, corresponding to a measured mass of 0.8 kg based on measurement.

Leather as a by-Product: Material inputs for the manufacture of cow leather tanned with a chromium process from the Ecoinvent database and shown in **Table S4.** According to the database, the inventory assumes the hides are a byproduct of milk and meat production without significant value, and therefore neglects the inputs of 989 kg of food and 0.56 ha of grassland per cow, based on average data from the Netherlands. Since less than 10% of revenue of cattle comes from by-products, with leather accounting for the majority of this revenue, a by-product model is compared in Figure 6.[12]

Leather as a co-Product: This inventory starts with the production of hides and skins as a co-product from beef cattle at a slaughterhouse. The dataset includes (portions of) the following

process: cattle raising, slaughtering, preservation of hides, chrome tanning, and finishing of chrome tanned leather. The allocation model used for the production of hides is economic allocation for the slaughterhouse. The inputs and outputs for subsequent processes, which includes preservation of hides, tanning, and finishing is based on Joseph and Nithya, 2008.[13] The majority of chrome tanning occurs in India, so energy processes for India have been used. Synthetic tans used for tanning is assumed to be a combination of DHDPS and formaldehyde.

Woven Cotton

Data from US-EcoInvent 2.0 is used to model the manufacture of 1 m^2 of medium weight (250 g/m^2) woven cotton farmed in the U.S., and includes: cotton fiber production, yarn production and weaving processes. The inventory includes the processes of soil cultivation, sowing, weed control, fertilization, pest and pathogen control, irrigation, harvest and ginning. Machine infrastructure and a shed for machine sheltering is included. Inputs of fertilizers, pesticides and seed as well as their transports to the farm, and the direct emissions on the field are also included. The system boundary is at the farm gate. Inputs are based on average production in the USA based on data collected in the period 2001-2006.Water for irrigation is pumped from 48 meter depth by electric pumps. Production of yarn from ginned fibers and weaving of cotton yarn into a textile are also included. The manufacturing impacts are shown in **Table S4**.

Microbial Cellulose biotextiles

$Biotextile_{LAB}$:

The system bill of materials was created from the Ecoinvent data sets and shown in **Table S6**. The biosynthesis cultivation media to biofabricate 1m^2 of microbial cellulose included 1.74 kg of sugar, 120 grams of green tea, 30 liters of water and 3864.68 Btu of heat energy from a natural gas boiler needed to raise the temperature of 15 liters of water from 25 C to 90 C ($Q=mc\Delta T$) to steep the tea and dissolve the sugar used in the cultivation media. Half the total water used in the liquid media (15 liters) is heated, the other half is added at room temperature to cool the media to a sufficiently low temperature (38 C or less) before adding 10% v/v starter culture to the media. The Ecoinvent data set for sugar included production of sugar from sugarcane and manufacturing at the sugar refinery. Impacts for production of 120 grams of tea used to produce 1 m^2 microbial cellulose were calculated based on APOS, U (of project Ecoinvent 3 {LK}) data for 1 kg tea, which includes farm cultivation, including irrigation, land use, field spraying insecticides and fertilizers (ammonium nitrate, ammonium sulfate,

glyphosate, diammonium phosphate production, drying and processing. Material inputs for the lecithin tanning emulsion (LT) included 0.28 kg of sunflower oil and 2 liters of distilled water to prepare the emulsion, and another liter of water to rinse after tanning. The sunflower seed oil data set included sunflower seed production and oil mill process. Phosphatidylcholine (lecithin powder) is produced as a byproduct from the edible oil industry, and as such, impacts are considered accounted for in the data set for sunflower seed oil, and is not available as a separate material input.

Biotextile$_{BP}$: Purification and Processing (LT) of 1 m2 of kombucha fermentation by-product (symbiotic colony of bacteria and yeast (SCOBY)).

The system of materials was based on the Ecoinvent data set and shown in **Table S7**. In the purification process of the MC in the form of a symbiotic colony of bacteria and yeast (SCOBY) provided by OM Champagne Tea, 8 liters of water and the heat energy to rise to 85C were utilized. The material inputs for the lecithin tanning process included 200 ml sunflower seed oil and 2 liters of water to tan 1m^2 of microbial nanocellulose biotextile.

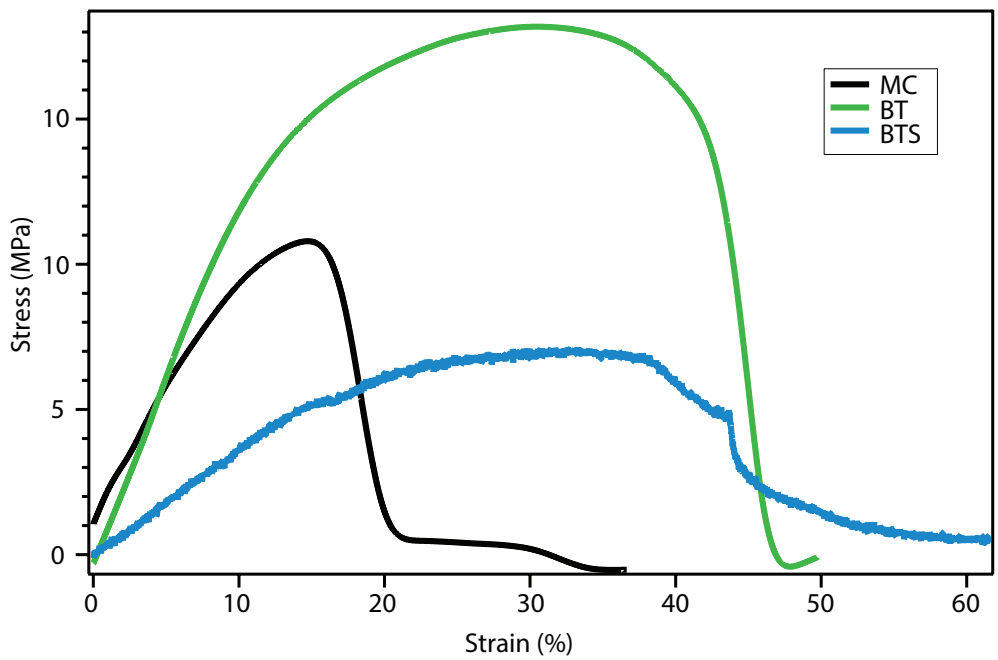

Figure S1
Stress-strain curves for brain tanned (BT) and brain tanned and smoked (BTS) microbial nanocellulose (MC), following ancient tanning practices, compared to as fabricated MC control, which encouraged the line of investigation in this work.

	Element Mass (%, n=3)	
Element	MC	LT
Carbon	74.68 ± 2.76	75.82 ± 1.91
Oxygen	21.20 ± 2.60	19.73 ± 1.97
Nitrogen	3.00 ± 1.16	0.56 ± 0.26
Phosphorus	0.57 ± 0.18	2.02 ± 0.18
Potassium	0.26 ± 0.05	1.71 ± 0.12
Sulfur	0.25 ± 0.07	0.12 ± 0.03
Copper	0	0
Sum	100	100

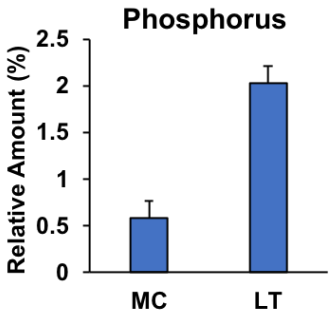

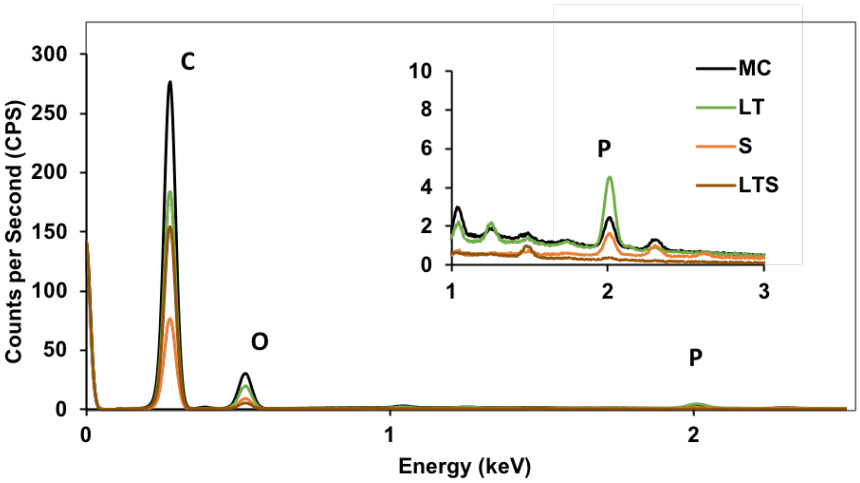

Figure S2
Energy dispersive x-ray measurements (^p<0.05, n=3) showing variation in chemical composition for the SEM micrographs in Figure 2A.

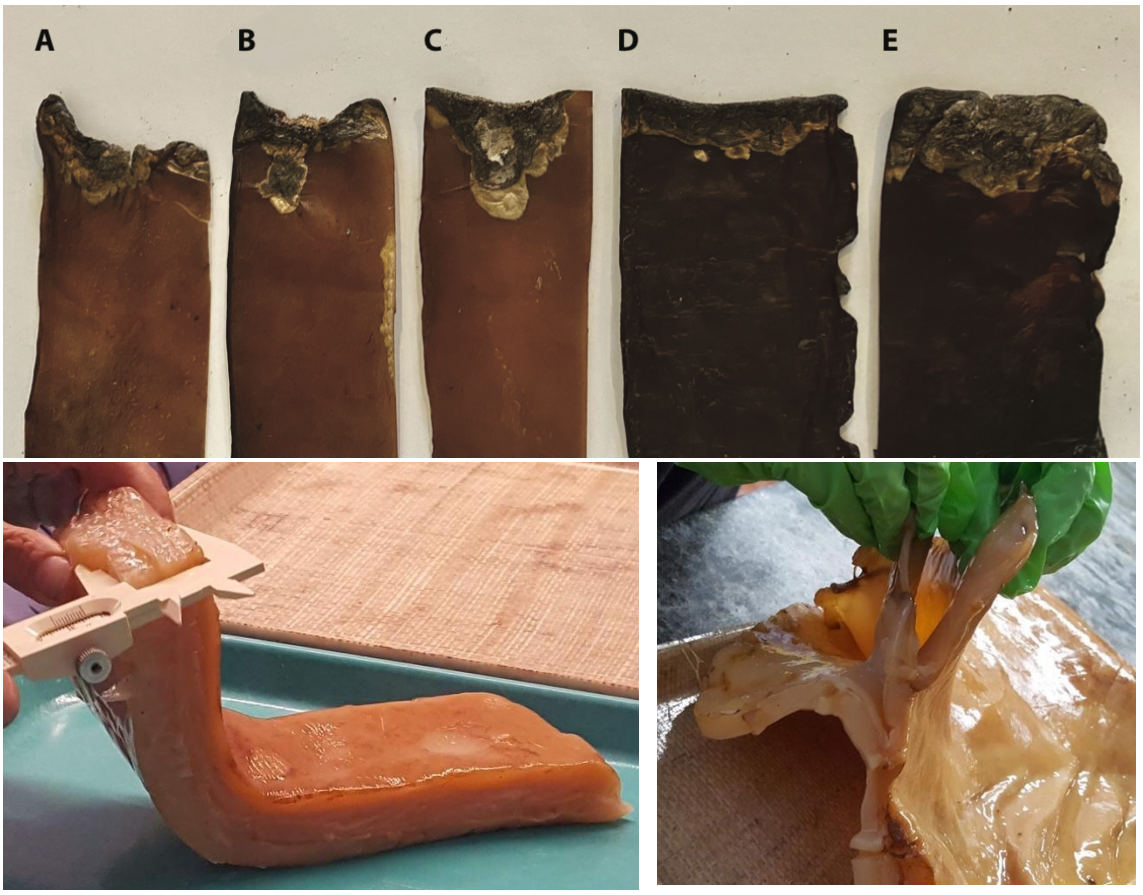

Figure S3
Top: Flame resistance as a function of MC biofilm thickness (layers) measured in the hydrated state from a single pellicle separated into layers: A) 0.3 cm; B) 0.7 cm; C) 1.0 cm; D) 2.2 cm; and E) 2.5 cm. **Bottom**: Cut sections of hydrated pellicle (**left**: **(E)** 2.5 cm thick) and separated into layer of varying thickness (**right: (A-C)** for flame studies).

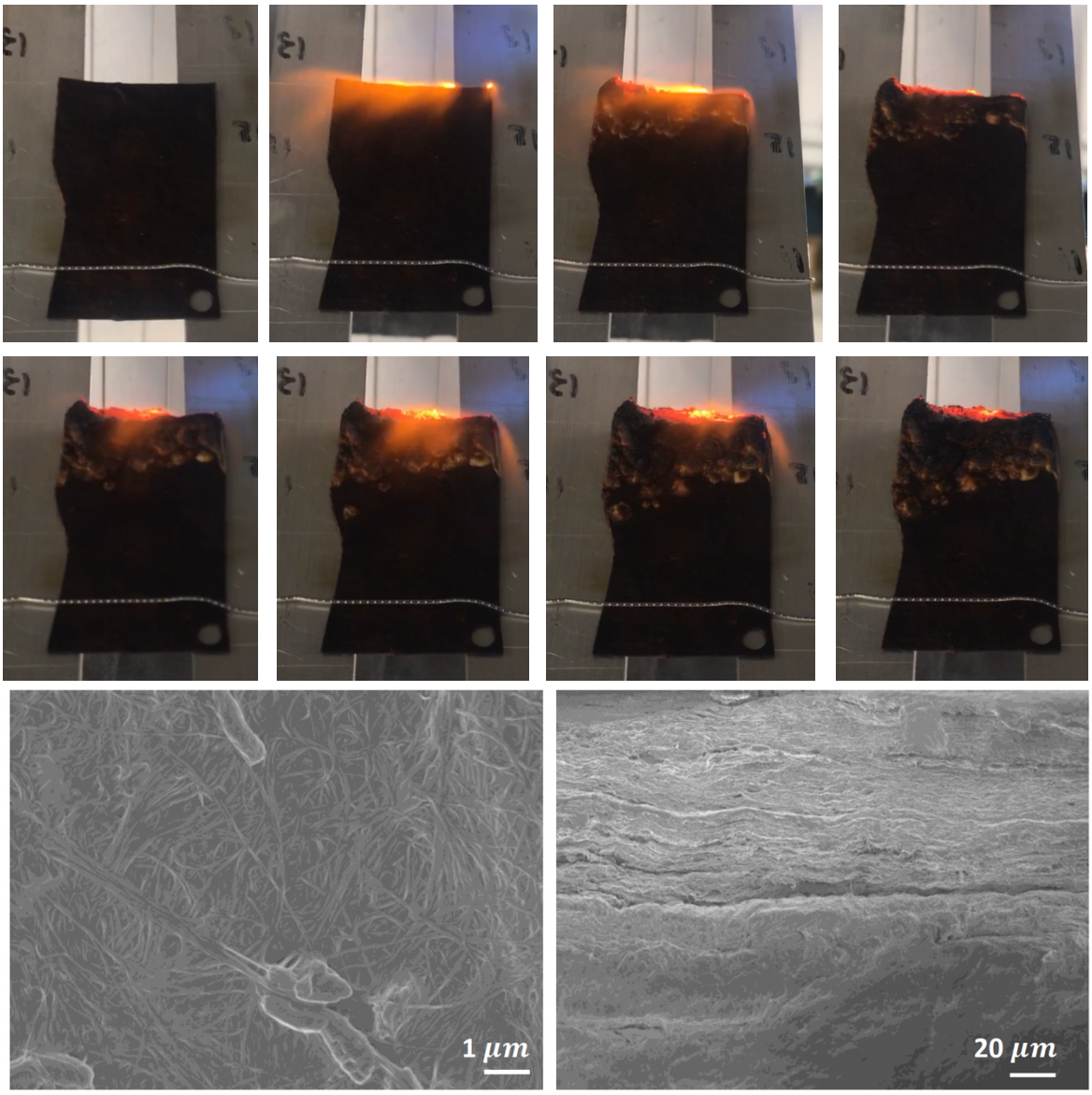

Figure S4
A) Flame testing of a cast slurry of MC, creating by blending MC pellicles in a Vitamix 3 HP blender and casting a 1.6 cm layer on a screen to dry in under ambient conditions. **B)** SEM images of untreated MC slurry surface **(left)** and cross-section **(right)** showing the blended MC self-organized into a layered structure, which as for the as grown MC films, imbues the material with a degree of flame retardance unique to microbial cellulose (as compared to plant cellulose).

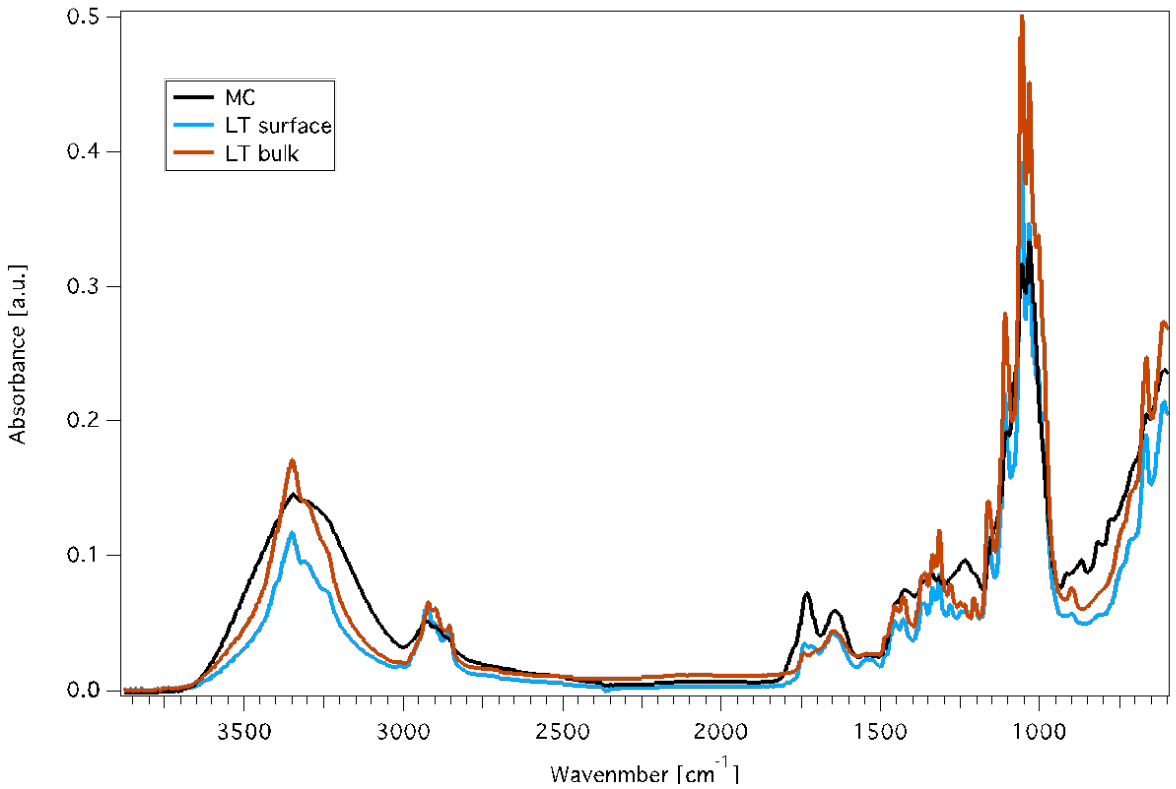

Figure S5

Fourier Transform Infrared Spectroscopy (FTIR) of as fabricated (MC) and lecithin tanned (LT) microbial cellulose, showing chemical changes are observed throughout the bulk of the biotextile. Bulk data was obtained by slicing hydrated LT samples in half before drying and exposing the face of the sample corresponding to the bulk region to the FTIR beam.

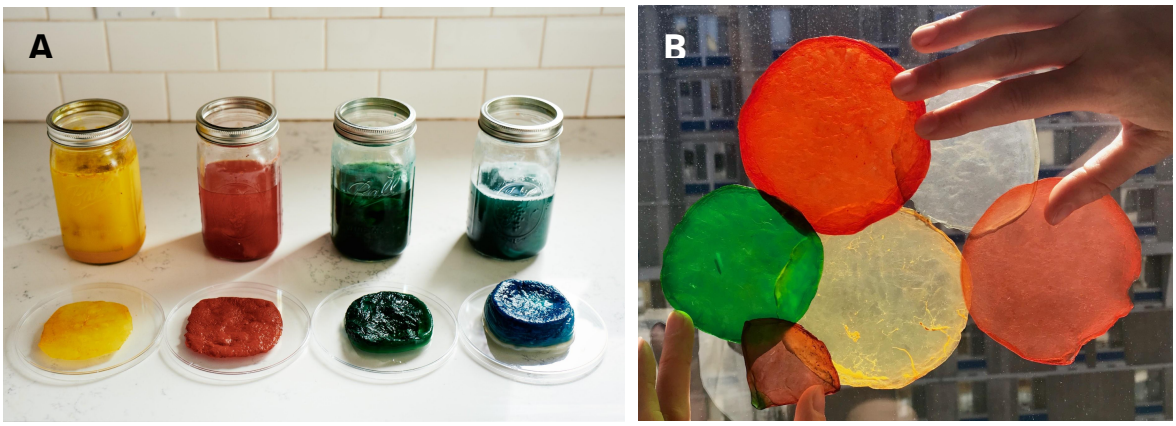

Figure S6
A) Examples of MC pellicles with color incorporated during microbial biosynthesis, using turmeric (yellow), cochineal (red), chlorophyll (green), and blue food coloring. **B)**: Examples of naturally dyed MC biotextiles after dehydration, including a transparent white obtained by immersion of MC in 0.5 M NaOH for one hour, followed by rinse in distilled water until reaching a neutral pH. See methods for details.

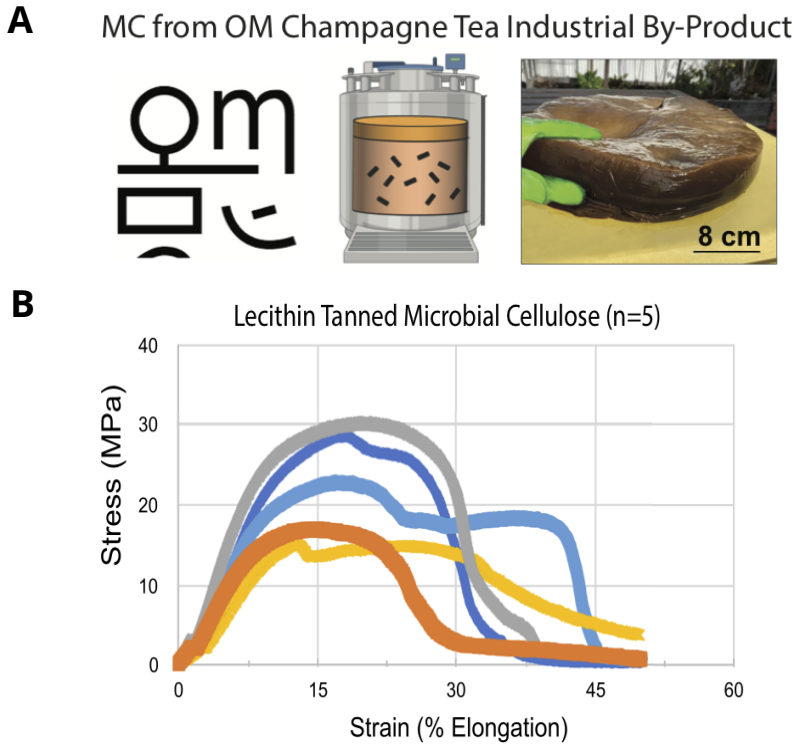

C

Sample	Thickness (mm)	Width (mm)	Area (mm^2)	Young's Modulus (MPa)	Max Stress (MPa)	Yield Strength (MPa)	Resilience (MPa)	Toughness (MPa)
1	1.55	12.70	19.69	213.71	17.13	12.21	0.37	3.75
2	1.38	12.70	17.53	341.44	30.21	20.59	0.67	7.69
3	1.60	12.70	20.32	172.59	15.17	12.34	0.47	4.95
4	1.52	12.70	19.30	271.54	22.95	15.50	0.49	7.44
5	1.19	12.70	15.11	298.06	28.90	19.44	0.70	6.39
Avg	1.45	12.70	18.39	259.47	22.87	16.02	0.54	6.04
STD	0.17	0.00	2.1	67.08	6.76	3.90	0.14	1.67

Figure S7
A) Microbial cellulose obtained as a by-product from commercial kombucha fermentation, provided by OM Champagne Tea, Mount Kisco, NY, corresponding to biotextile 2 in Figure 6 and the LCA analysis. Mechanical tensile data (n=5) after lecithin tanning and drying under ambient conditions expressed as: **B)** stress-strain curves; and **C)** specific parameters including modulus, max strength, yield strength, resilience and toughness.

CS (crystallite size (nm)) L[200]					CS (crystallite size (nm)) L[101]			
n	**MC**	**LT**	**LTS**	**Smoked**	**MC**	**LT**	**LTS**	**Smoked**
1	6.371	6.652	6.489	7.482	4.694	4.970	4.937	5.006
2	6.702	6.646	6.571	5.826	4.777	4.943	4.987	4.852
3	6.472	7.165	6.349	5.912	4.774	4.927	4.853	4.844
4	6.559	6.517	6.276	6.327	4.751	4.870	4.910	4.827
5	6.604	6.433	6.514	7.380	4.824	4.949	4.867	4.958
Average:	**6.542**	**6.683**	**6.440**	**6.585**	**4.764**	**4.932**	**4.911**	**4.897**
STD	0.127	0.285	0.123	0.796	0.047	0.038	0.054	0.080

n=5	**d-spacing [200] (nm)**	**d-spacing [101] (nm)**
MC	0.60± 0.003	0.39 ± 0.001
LT	0.61 ± 0.001	0.39 ± 0.001
LTS	0.60 ± 0.031	0.39 ± 0.0011
S	0.60 ± 0.008	0.39 ± 0.0034

Table S1
Crystallite size (CS) and d-spacing in nm along the [200] and [101] planes for microbial nanocellulose before and after lecithin and aldehyde treatment, obtained from X-ray diffraction (XRD) Bragg peaks, where d_i is the initial lattice spacing, d_f is the final lattice spacing, with d calculated according to Bragg's Law: $\lambda = 2d_{hkl}*\sin\theta$ and $CS=k\lambda/(FWHM*\cos\theta)$, where k=0.9 is the correction factor, λ=1.54056 Å is the x-ray wavelength, FWHM is the full-width at half maximum of the Bragg peak, and θ is the diffraction angle, as described in Methods.

Peak Intensities [a.u.]	MC	LT surface	LT bulk
A_{897}	0.066	0.067	0.077
A_{1375}	0.068	0.072	0.086
A_{1430}	0.056	0.061	0.072
A_{2917}	0.081	0.068	0.067
IR Crystallinity Ratio	**MC**	**LT surface**	**LT bulk**
TCI (A_{1372}/A_{2900})	0.840	1.059	1.28
LOI (A_{1429}/A_{897})	0.849	0.911	0.935
Absorbance Ratio (A_{2917})			
A_{897}	0.815	0.985	1.149
A_{1375}	0.840	1.058	1.2844
A_{1430}	0.691	0.897	1.075

Table S2
Total Crystallinity Index (TCI), Lateral Order Index (LOI) and absorbance ratio for the peaks relative to A_{2917} used to probe hydrogen bond intensity (HBI) obtained from FTIR data. The data shows a slight in crystallinity, order, and decrease in hydrogen bonding due to formation of chemical cross-links (phosphates, methylene and carboxyl groups) with lecithin tanning (LT compared to as-fabricated MC) throughout the bulk of the samples.

Impact category	Normalization	Unit	Weighting (%)
Ozone depletion	1.61E-01	kg CFC^{-11} eq /year /capita	2.40E+00
Global warming	2.42E+04	kg CO_2 eq /year /capita	3.49E+01
Smog	1.39E+03	kg O_3 eq /year /capita	4.80E+00
Acidification	9.09E+01	kg SO_2 eq /year /capita	3.60E+00
Eutrophication	2.16E+01	kg N eq /year /capita	7.20E+00
Carcinogenics	5.07E-05	CTUh /year /capita	9.60E+00
Non-carcinogenics (Hormonally active agents (HAA))	1.05E-03	CTUh /year /capita	6.00E+00
Respiratory effects	2.43E+01	kg PM2.5 eq /year /capita	1.08E+01
Ecotoxicity	1.10E+04	CTUe /year /capita	8.40E+00
Fossil fuel depletion	1.73E+04	MJ surplus /year /capita	1.21E+01

Table S3
LCA normalization and weighting factors used to convert specific impacts to an impact factor expressed in mPts per functional unit (here 1 m^2 of textile).

Textile	Leather (By-product)	Leather (Co-product)	PU textile	Cotton	$Biotextile_{LAB}$	$Biotextile_{BP}$
Mass/m^2 (kg)	0.8	N/A (inputs/m^2)	0.66	0.25	N/A (inputs/m^2)	N/A (inputs/m^2)
Material inventory	Cow leather (hides, chromium process)	Cow leather (slaughter house, hides, chromium process)	59.4 g epoxy resin 9.9 g ethyl acetate 1g citric acid, 11.55 g N,N-dimethylformamide 594 g polyester fabric	Cotton fibers, yarn, woven textile	40 liters water 120 g green tea 296 ml sunflower seed oil 1740 g sugar 1744 Btu natural gas heat	10 liters water 296 ml sunflower seed oil 3864.68 Btu natural gas heat
Additional processes	N/A	N/A	N/A	Fiber production and ginning, yarn production, weaving	N/A	N/A
Impact category						
Total Impacts (mPts)	**3.82**	**989**	**0.62**	**0.47**	**0.30**	**9.63E-02**
Acidification	2.1E-03	0.62	3.2E-02	2.32E-02	2.74E-03	5.75E-04
Ecotoxicity	1.5E-02	39.1	3.1E-02	0.06	4.88E-02	2.05E-02
Eutrophication	3.9E-04	3.36	3.5E-02	3.66E-02	5.55E-02	5.06E-02
Global warming	**1.7E-02**	**1.85**	**0.166**	**9.37E-02**	**1.3E-02**	**5.29E-03**
Ozone depletion	1.9E-05	8.0E-04	1.3E-04	2.38E-05	1.75E-05	8.28E-06
Fossil fuel depletion	1.4E-02	0.64	0.12	1.60E-02	9.42E-03	4.09E-03
Carcinogenics	**3.63**	**937**	**0.16**	**0.146**	**6.85E-02**	**7.07E-03**
Non-carcinogenics (HAA)	2.8E-03	5.78	2.4 E-02	5.11E-02	8.75E-02	7.00E-03
Respiratory effects	1.4E-03	0.6	1.0 E-02	2.52E-02	6.67E-03	1.00E-03
Smog	1.7E-03	0.19	4.5E-02	1.67E-02	2.80E-03	8.06E-05
CO_2 eq. (kg)	**1.17**	**128**	**11.50**	**6.50**	**0.89**	**0.37**

Table S4
Cradle to Gate LCA - Manufacturing Impacts for 1 m^2 of textile. Values obtained from LCA based within the Sustainable Minds software using the Ecoinvent data sets described.

Input	Polyester (PET)	Epoxy resin	Ethyl acetate	Citric acid	DMF
Total impacts	**0.58**	**3.4E-02**	**2.39E-03**	**6.0E-04**	**9.81E-03**
Acidification	3.08E-02	1.04E-03	5.29E-05	1.70E-05	5.86E-05
Ecotoxicity	2.86E-02	2.34E-03	1.02E-04	1.18E-04	1.04E-04
Eutrophication	2.60E-02	8.86E-04	1.32E-04	3.38E-05	7.8E-03
Global warming	0.159	5.76E-03	4.62E-04	8.76E-05	3.87E-04
Ozone depletion	1.27E-04	1.52E-08	6.10E-07	1.16E-07	6.76E-07
Fossil fuel depletion	0.113	6.33E-03	6.53E-04	3.32E-05	4.89E-04
Carcinogenics	0.145	1.1E-02	7.42E-04	2.15E-04	7.45E-04
Non-carcinogenics /HAA	2.10E-02	3.02E-03	1.36E-04	5.64E-05	1.32E-04
Respiratory effects	8.41E-03	1.76E-03	4.62E-05	2.46E-05	4.85E-05
Smog	4.30E-02	1.78E-03	4.94E-05	1.43E-05	4.25E-05
CO_2 eq. (kgs)	**11.0**	**0.4**	**0.032**	**6.1E-03**	**2.68E-02**

Table S5
Impacts for 1 m^2 of polyurethane (PU)-coated polyester textile (synthetic leather) by input computed within the LCA methodology (Figure 6).

Input	Fiber production	Yarn production	Weaving process
Total impacts	**0.13**	**0.15**	**0.19**
Acidification	2.56E-03	8.96E-03	1.16E-02
Ecotoxicity	4.47E-02	6.23E-03	7.62E-03
Eutrophication	3.35E-02	1.34E-03	1.73E-03
Global warming	9.0E-03	3.76E-02	4.71E-02
Ozone depletion	8.22E-06	7.55E-06	8.01E-06
Fossil fuel depletion	4.47E-03	5.44E-03	6.12E-03
Carcinogenics	1.65E-02	5.85E-02	7.1E-02
Non carcinogenics	1.67E-02	1.5E-02	1.94E-02
Respiratory effects	2.13E-03	9.93E-03	1.32E-02
Smog	2.0E-03	6.35E-03	6.35E-03
CO_2 eq. (kgs)	**0.625**	**2.61**	**3.27**

Table S6
Impacts for 1m^2 of cotton fabric by input computed within the LCA methodology.

Input	Sugar	Sunflower seed oil	Green tea	Natural gas	Tap water
Inventory	1.74 kg	296 ml	120 g	3864.7 Btu	40 l
Total Impacts	**0.192**	**1.92E-02**	**1.24E-04**	**1.04E-02**	**1.34E-03**
Acidification	2.08E-03	5.17E-04	1.42E-06	1.04E-04	4.32E-05
Ecotoxicity	2.82E-02	2.05E-02	5.50E-05	4.99E-05	6.85E-05
Eutrophication	4.85E-03	5.06E-02	1.15E-05	3.4E-05	8.51E-06
Global warming	5.08E-03	3.31E-03	2.95E-06	4.23E-03	2.51E-04
Ozone depletion	5.12E-6	4.92E-6	2.43E-09	7.38E-06	1.29E-07
Fossil fuel depletion	2.65E-03	1.91E-03	1.40E-06	4.79E-03	7.28E-05
Carcinogenics	6.04E-02	6.49E-03	1.95E-05	8.77E-04	7.17E-04
Non-carcinogenics /HAA	8.04E-02	6.93E-03	3.08E-05	1.01E-04	1.13E-04
Respiratory effects	5.61E-03	9.64E-04	1.21E-06	6.07E-5	3.65E-05
Smog	2.61E-03	1.11E-06	5.55E-07	1.59E-04	3.10E-05
CO_2 eq. (kg)	**0.353**	**0.229**	**2.05E-02**	**0.294**	**1.74E-02**

Table S7
Cradle to Gate LCA -Biotextile$_{LAB}$- Impacts for laboratory scale biosynthesis and lecithin tanning of 1 m^2 of LT MC textile by input.

Input	Tap water	Natural gas (boiler modulating >100kW)	Sunflower seed oil
Total Impacts	**3.35E-04**	**4.71E-03**	**9.12E-02**
Acidification	1.08E-05	4.67E-05	5.17E-04
Ecotoxicity	1.71E-05	2.25E-05	2.05E-02
Eutrophication	2.13E-06	1.54E-05	5.06E-02
Global warming	6.27E-05	0.00192	3.31E-03
Ozone depletion	3.22E-08	3.33E-06	4.92E-6
Fossil fuel depletion	1.82E-05	2.16E-03	1.91E-03
Carcinogenics	1.79E-04	3.96E-04	6.49E-03
Non-carcinogenics /HAA	2.82E-05	4.57E-05	6.93E-03
Respiratory effects	9.12E-06	2.74E-05	9.64E-04
Smog	7.75E-06	7.17E-05	1.11E-06
CO_2 eq. (kg)	**4.35E-03**	**0.133**	**0.229**

Table S8
Cradle to Gate LCA -Biotextile$_{BP}$- Impacts for 1 m^2 of biotextile fabricated using microbial nanocellulose side streams from kombucha fermentation, by input.

Sample (n=5)	Initial mass (g) Day 0	Final mass (g) Day 60	Mass loss (%)	Average mass loss (%)
MC 1	0.09	0.024	73.33	
MC 2	0.09	0.02	77.78	
MC 3	0.09	0.025	72.22	
MC 4	0.09	--	--	
MC 5	0.09	--	--	
MC				**74.45 +/- 2.94**
LT 1	0.05	0.013	74	
LT 2	0.04	0.012	70	
LT 3	0.04	0.009	77.5	
LT 4	0.04	0.008	80	
LT 5	0.04	0.008	80	
LT				**76.30+/- 4.30**

Table S9
Biodegradation in natural terrestrial environment of 2 x 2 cm samples (n=5) of as fabricated (MC) and lecithin tanned (LT) microbial biotextiles evaluated as mass lost after 60 days outdoors in soil. Two of the MC samples were not found upon retrieval. The slightly larger mass loss for LT is likely due to the lower density (thickness of the MC nanofiber mesh) of the samples relative to MC (0.0105 g/cm^2 vs 0.0225 g/cm^2).

Microbial Cellulose Biosynthesis Time Lapse

Movie S1

Time lapse of microbial cellulose biosynthesis over 21 days at 24°C using: **A)** sucrose and **B)** fructose as carbon sources shows tunable and scalable biosynthesis highlighting the ability of *G. Xylinum* to utilize a variety of nutrient sources in its carbon metabolism.

Movie S2

Water repellency of waxed MC biotextile

References

[1] I.V. Muralikrishna, V. Manickam, Life Cycle Assessment in *Environmental Management* (Butterworth-Heinemann, Oxford, United Kingdom, 2017), pp. 57–75
[2] M. Ryberg, M.D.M. Vieira, M. Zgola, M. J. Bare, R. K. Rosenbaum, Updated US and Canadian Normalization Factors for TRACI 2.1. *Clean Techn. Environ. Policy* **16**, 329–339 (2014).
[3] http://www.sustainableminds.com/showroom/shared/learn-single-score.html
[4] T.P. Gloria, B.C. Lippiatt, J. Cooper, Life Cycle Impact Assessment Weights to Support Environmentally Preferable Purchasing in the United States. *Environ. Sci. Technol.* 41, 21, 7551–7557 (2007).
[5] Synthetic Leather Market Size, Share & Trends Analysis Report By Product (Bio-based, PVC, PU), By Application (Clothing, Furnishing, Automotive, Bags & Wallets, Footwear), By Region, And Segment Forecasts, 2020 - 2027 https://www.grandviewresearch.com/industry-analysis/synthetic-leather-market
[6] International Trade Centre, http://www.intracen.org/itc/sectors/leather/
[7] Market Size, Share & Trends Analysis Report By Raw Material (Wool, Chemical, Silk, Cotton), By Product (Natural Fibers, Polyester, Nylon), By Application, By Region, And Segment Forecasts, 2020 - 2027 - https://www.grandviewresearch.com/industry-analysis/textile-market
[8] Synthetic Leather (Artificial Leather) Market by Type (Polyurethane, Polyvinyl Chloride, Bio-based), End-Use Industry (Footwear, Furnishing, Automotive, Clothing, Bags, Purses & Wallets, Sports, Electronics) - Global Forecast to 2021. https://www.marketsandmarkets.com/Market-Reports/synthetic-leather-market-6616309.html
[9] Clarino Crust Technical Sheet. Status September 2018. https://www.clarino.eu/fileadmin/user_upload/CLARINO/technical_data_sheets/clarino_crust/Clarino_Crust.pdf
[10] Heshan Xinkeda Enterprises Co Ltd. The urethane composition of use for synthetic leather. China CN105255155B, filed October 10, 2015 and granted February 6, 2018.
[11] A.K. Sen, Textile Substrate for Coated Fabrics and Non-Apparel Coating in *Coated Textiles - Principles and Applications*, 2nd Edition, CRC Press, Boca Raton, FL, USA, pp. 64; 147 (2008).
[12] https://www.ers.usda.gov/webdocs/outlooks/37427/8801_ldpm20901.pdf

[13] K. Joseph, N. Nithya. Material flows in the life cycle of leather, *J. Clean. Prod.* **17**, 7, 676-682 (2009).